



Creation and Evolution of Impact-generated Reduced Atmospheres of Early Earth

Kevin J. Zahnle¹ , Roxana Lupu² , David C. Catling³ , and Nick Wogan³ ¹ Space Science Division, NASA Ames Research Center, Mail Stop 245-3, Moffett Field, CA 94035, USA; Kevin.J.Zahnle@nasa.gov² BAER Institute, NASA Ames Research Center, Moffett Field, CA 94035, USA; Roxana.E.Lupu@nasa.gov³ Dept. of Earth and Space Sciences, University of Washington, Seattle, WA 98195, USA; dcating@u.washington.edu

Received 2019 December 31; revised 2020 February 7; accepted 2020 February 10; published 2020 May 1

Abstract

The origin of life on Earth seems to demand a highly reduced early atmosphere, rich in CH₄, H₂, and NH₃, but geological evidence suggests that Earth's mantle has always been relatively oxidized and its emissions dominated by CO₂, H₂O, and N₂. The paradox can be resolved by exploiting the reducing power inherent in the “late veneer,” i.e., material accreted by Earth after the Moon-forming impact. Isotopic evidence indicates that the late veneer consisted of extremely dry, highly reduced inner solar system materials, suggesting that Earth's oceans were already present when the late veneer came. The major primary product of reaction between the late veneer's iron and Earth's water was H₂. Ocean-vaporizing impacts generate high pressures and long cooling times that favor CH₄ and NH₃. Impacts too small to vaporize the oceans are much less productive of CH₄ and NH₃, unless (i) catalysts were available to speed their formation, or (ii) additional reducing power was extracted from pre-existing crustal or mantle materials. The transient H₂–CH₄ atmospheres evolve photochemically to generate nitrogenated hydrocarbons at rates determined by solar radiation and hydrogen escape, on timescales ranging up to tens of millions of years and with cumulative organic production ranging up to half a kilometer. Roughly one ocean of hydrogen escapes. After the methane is gone, the atmosphere is typically H₂- and CO-rich, with eventual oxidation to CO₂ rate-limited by water photolysis and hydrogen escape.

Unified Astronomy Thesaurus concepts: Earth (planet) (439); Earth atmosphere (437); Astrobiology (74); Pre-biotic astrochemistry (2079); Atmospheric composition (2120)

1. Introduction

The modern science of the origin of life on Earth begins with Haldane (1929) and Oparin (1938). Both argued that a highly reduced early terrestrial environment—profoundly unlike the world of today, even with O₂ removed—was needed. Oparin's specific emphasis on methane, ammonia, formaldehyde, and hydrogen cyanide as primordial materials suitable for further development remains a recurring theme in origin-of-life studies (Urey 1952; Oró & Kamat 1961; Ferris et al. 1978; Stribling & Miller 1987; Oró et al. 1990; Ricardo et al. 2004; Powner et al. 2009; Sutherland 2016; Benner et al. 2019a). Although some of these materials—formaldehyde in particular—can be generated under weakly reducing conditions (Pinto et al. 1980; Benner et al. 2019b), others (such as cyanamide and cyanoacetylene) require strongly reducing conditions. The hypothesized reducing atmosphere inspired the famous and often-replicated Miller–Urey experiments, in which sparked or UV-irradiated gas mixtures spontaneously generate a wide range of organic molecules (Miller 1953, 1955; Miller & Urey 1959; Cleaves et al. 2008; Johnson et al. 2008).

The geological argument against a reducing early atmosphere is nearly as old (e.g., Poole 1951), although often accompanied by the caveat that things could have been different before the rock record (e.g., Holland 1964, 1984; Abelson 1966; Walker 1977). The underlying presumption is that the atmosphere should have resembled volcanic gases. Modern volcanic gases are roughly consistent with the quartz-fayalite-magnetite (QFM) mineral buffer, for which the redox

state is determined by chemical reactions between ferrous (Fe⁺²) and ferric iron (Fe⁺³). At typical magma temperatures, QFM predicts that H₂ and CO would be present at percent levels compared to H₂O and CO₂, and that methane and ammonia would be negligible.

Some studies suggest that the Archean mantle had a similar redox state to today (Delano 2001; Canil 2002; Rollinson et al. 2017), while rare earth elements in zircons suggest a Hadean mantle consistent with QFM (Trail et al. 2012). Large uncertainties in observationally derived oxygen fugacities (± 2 in log₁₀(*f*_{O₂})) may obscure a secular trend, while some simplifying assumptions made in earlier *f*_{O₂} studies are open to question (Wang et al. 2019). (The redox state of rocks is usually described by oxygen fugacity *f*_{O₂}, which describes the formal abundance of O₂ gas in units of atmospheres.) Two recent studies that use filtered samples hint that log₁₀(*f*_{O₂}) of the mantle increased by ~1.3 from the early Archean to Proterozoic (Aulbach & Stagno 2016; Nicklas et al. 2019).

Concurrently, a body of experimental evidence has accumulated suggesting that ferrous silicates in Earth's mantle disproportionate under great pressure into ferric iron and metallic iron, with the latter expected to migrate to the core (Frost & McCammon 2008). This would leave the mantle, or at least part of the mantle, in a QFM-like state of oxidation from the time our planet first became big enough to be called Earth (Armstrong et al. 2019).

Given the incompatibility of a QFM mantle with a reduced atmosphere, workers have turned to impact degassing, in which gases are directly released into the atmosphere on impact (Matsui & Abe 1986; Tyburczy et al. 1986; Ahrens et al. 1989). Most impactors are much more reduced than the mantle and often better endowed (gram per gram) in atmophile elements (Urey 1952; Hashimoto et al. 2007; Schaefer & Fegley 2007;



Original content from this work may be used under the terms of the [Creative Commons Attribution 4.0 licence](https://creativecommons.org/licenses/by/4.0/). Any further distribution of this work must maintain attribution to the author(s) and the title of the work, journal citation and DOI.

Sugita & Schultz 2009). Many meteorites, including ordinary chondrites and enstatite chondrites, contain substantial amounts of metallic iron and iron sulfides. Gases that equilibrate with these highly reduced meteoritic materials would be highly reduced themselves (Kasting 1990; Hashimoto et al. 2007; Schaefer & Fegley 2007, 2010, 2017; Kuwahara & Sugita 2015), provided that there is enough iron to reduce all of the atmophiles in the impactor. But if there are more atmophiles to reduce than iron to reduce them, the gas composition can evolve to a much more oxidized state (Schaefer & Fegley 2017).

Several of the new impact-degassing studies (Hashimoto et al. 2007; Schaefer & Fegley 2007, 2010, 2017) calculate gas compositions in equilibrium with mineral assemblages at fixed pressures, with temperature treated as an independent variable. These calculations often promise big yields of CH₄ and NH₃ at low temperatures. However, actual yields depend on the quench conditions in the gas as it cools after the impact. A cooling gas is said to have quenched when the chemical reactions maintaining equilibrium between species become so sluggish that the composition of the gas freezes (Zel'dovich & Raizer 1967). Quenching is mostly determined by temperature. Gas-phase reactions for making CH₄ from CO are strongly inhibited by low temperatures, and those for making NH₃ from N₂ are even more strongly inhibited. So unless an abundant catalyst were available to lower the effective quench temperature (Kress & McKay 2004), there is a tendency for the shock-heated gas to quench to CO, N₂, and H₂. Of the new studies, only Kuwahara & Sugita (2015) have attempted to calculate quench conditions, but their results are problematic because they used the entropy of shocked silica to estimate the entropy of shocked carbonaceous chondrites, which results in artificially low temperatures and artificially large amounts of methane. Finally, in a full account, the quenched plume of impact gases would be mixed into, and diluted by, the pre-existing atmosphere.

This study follows the lead of Genda et al. (2017a, 2017b) and Benner et al. (2019a) in addressing how the largest cosmic impacts changed the ocean and atmosphere that were already present on Earth. We go beyond Genda et al. (2017a, 2017b) and Benner et al. (2019a) in addressing not just the single largest impact but also a full range of sizes, extending to impacts 100 and even 1000 times smaller (Hadean Earth would have experienced scores of these). Our particular focus is on impacts that process the entire atmosphere and hydrosphere. This differs from previous studies of smaller impacts that find that the main product of impact is HCN, and this occurs only in atmospheres with C/O ratios greater than unity (Chyba & Sagan 1992). Section 2 provides a brief summary of impacts after the Moon formed as constrained by geochemistry and the craters of the Moon. Section 3 addresses impact-generation of methane-rich atmospheres on Earth. The emphasis is on impacts that are big enough to vaporize the oceans, as these produce long-lasting hot conditions at high pressures and, thus, can be highly favorable to methane and sometimes even to ammonia. Section 4 uses a simple model to address the subsequent photochemical evolution of these atmospheres. The emphasis here is on the fate of methane and the production of organic material and hazes on the photochemistry of nitrogen and the generation of HCN and other nitrogenated organics, and on hydrogen escape. Ammonia is (mostly) deferred to the Discussion.

2. The Late Veneer

The highly siderophile elements (HSEs) comprise seven heavy metals (Ru, Rh, Pd, Os, Ir, Pt, and Au) with very strong tendencies to partition into planetary cores. If Earth's mantle and core were fully equilibrated, almost all of its HSEs would be in the core, and the tiny remnant in the mantle would be highly chemically fractionated (Walker 2009; Rubie et al. 2015, 2016; Day et al. 2016). But this is not what is seen. Rather, the mantle contains a modest cohort of excess HSEs that, to first approximation, are present in roughly the same relative abundances that they have in chondritic meteorites (Day et al. 2016). One explanation is that the excess HSEs were dropped into the mantle and left stranded there some time after core formation was complete. If the mantle's HSEs were added with other elements in chondritic proportions, they correspond to about 0.5% of Earth's mass (Anders 1989). The late-added mass carrying the HSEs is usually called the "late veneer."

The late veneer measured in this way is very big. Viewed literally, 0.5% of Earth's mass corresponds to a veneer 20 km thick. Gathered into a sphere, it corresponds to a rocky world 2300 km diameter—as big as Pluto, and more massive. We will call this the "maximum HSE" veneer. If the veneer were sourced from fragments of differentiated worlds, the veneer mass could be a little smaller or much bigger.

Historically, the late veneer was presumed volatile-rich, as would be expected if the last materials to fall to Earth fell from the cold distant outer solar system (Anders & Owen 1977; Wänke & Dreibus 1988; Dreibus et al. 1989; Marty 2012; Albarède et al. 2013; Halliday 2013). However, the late veneer now appears constrained by Ru isotopes to resemble either enstatite chondrites, enstatite achondrites (a.k.a., aubrites), or iron meteorites of type IAB and, thus, appears to come from the same deep inner solar system reservoir as Earth itself (Fischer-Gödde et al. 2015; Dauphas 2017; Fischer-Gödde & Kleine 2017; Birmingham et al. 2018; Carlson et al. 2018; Hopp & Kleine 2018). All of our samples of these materials are profoundly reduced and very dry. This apparently excludes the late veneer as the source of water on Earth (Fischer-Gödde & Kleine 2017; Carlson et al. 2018), and thus, the late veneer can be presumed to have impacted into an Earth already fully plished with oceans, a view also consistent with oxygen isotopes (Greenwood et al. 2018). The late veneer's role changes from water bearer to water changer: it must now be viewed as a source of reducing power injected into Earth's near-surface environment (Pasek & Lauretta 2008; Genda et al. 2017a, 2017b; Benner et al. 2019a).

The total reducing power delivered by the maximum late veneer can be illustrated by using all of its metallic iron to reduce water to hydrogen, in stoichiometry, $\text{Fe} + \text{H}_2\text{O} \rightarrow \text{FeO} + \text{H}_2$. The iron that accompanied the mantle's excess HSEs corresponded to 1×10^{25} g of metal. Because the HSEs remained in the mantle, neither they nor the iron that came with them went to the core, and thus, we can be confident that the iron was oxidized at the surface, in the crust, or in the mantle. There is enough iron in the late veneer to reduce 1.8×10^{23} moles of H₂O to H₂ and FeO, which corresponds to reducing of 2.3 oceans of water to hydrogen.

If the late veneer were characterized by size-number statistics typical of stray solar system bodies, it is likely that most of the mantle's HSE excess was carried by a single Pluto-sized body (Sleep et al. 1989; Tremaine & Dones 1993; Bottke et al. 2010; Brasser et al. 2016; Genda et al. 2017a).

Comparison with the uncertain but apparently much smaller lunar HSE excess (Day et al. 2016) is consistent with the conjecture that the maximum HSE event was singular (Brasser et al. 2016; Morbidelli et al. 2018); although, this is not required, as there are other ways of explaining the scarcity of lunar HSEs that do not imply different accretion rates for Earth and Moon (see Kraus et al. 2015).

But even if the late veneer were delivered by one body, it does not follow that its mass was added to Earth in a moment. There is a considerable likelihood, estimated as 50% by Agnor & Asphaug (2004), that an impact results not in a merger but rather in the disintegration of the smaller body. The debris are distributed in a ring around the Sun coincident with Earth's orbit and swept up by Earth over tens or hundreds of thousands of years (Genda et al. 2017a, 2017b). Few of the debris are swept up by the Moon, owing to the much greater gravitational cross section of Earth with respect to debris in quasi-circular orbits (Genda et al. 2017a). This kind of distributed event is likely to strand nearly all of its HSEs in the crust or at shallow depths in Earth's mantle, while the direct impact of a Pluto-sized body might be expected to drive much of the impactor's core directly into our own. Stranding *all* of the newly added HSEs in the mantle without fractionation fulfills a second independent requirement imposed by the mantle's Ru isotopes, which were not mass-fractionated by partitioning between the mantle and core (Fischer-Gödde & Kleine 2017; Hopp & Kleine 2018). Dividing the impactor into myriads of smaller particles would also be more effective at chemically reducing Earth's atmosphere and ocean. For example, Genda et al. (2017b) model a Moon-sized impactor and find that 60% of the iron would be divided into mm-size droplets. The overall picture resembles that suggested by Urey (1952), who wrote that "materials would have fallen through the atmosphere in the form of iron and silicate rains and would have reacted with the atmosphere (and hydrosphere) in the process."

An important caveat is that a maximum HSE impact may not couple well to the oceans. A Pluto-sized impact would blanket Earth in tens of kilometers of impact ejecta, which is so much deeper than the oceans that much of the iron may have been buried before it could react with water. Under these conditions, the buried iron would have remained unoxidized in the upper mantle for a considerable period of time. We know from the presence of the HSEs and the unfractionated Ru isotopes that the iron was not removed to the core. The iron must therefore have strongly influenced the redox state of volcanic gases until its oxidation was complete. The effect of this is to prolong the influence of the maximum HSE event to geological timescales.

There is also a small chance that the late veneer is an illusion. It has been suggested that Earth's HSE excess may date to the Moon-forming impact itself (Newsom & Taylor 1989; Brasser et al. 2016; Sleep 2016). If so, the mantle's HSE excess overestimates the amount of reducing power delivered to Earth after the Moon-forming impact. A crude lower bound on the late veneer can be extrapolated from the lunar crater record (Sleep et al. 1989; Zahnle & Sleep 1997, 2006). This scaling suggests that the "minimum late veneer" delivered between 3% and 30% of the mass as the maximum HSE veneer. The large uncertainty, and large total mass striking Earth compared to the Moon, both arise from the high probability that *all* of the largest bodies in a given population hit the Earth (Sleep et al. 1989).

Table 1 lists a representative sampling of maximum and minimum late veneer impacts. The number of bodies in any given size class is estimated from the cumulative relation $N(>m) \propto m^{-b}$, with $0.5 < b < 0.9$, with the smaller number based on the number of lunar basins and with the larger number based on the total cumulative mass of the maximum late veneer using methods described by Zahnle & Sleep (1997). The number of oceans that can be vaporized assumes that 50% of the impact energy is available to evaporate an ocean (1.4×10^{24} g) of water and heat the steam to 1500 K. The number of oceans that can be reduced to H₂ assumes an EH enstatite chondritic composition with 33% Feby mass and that the reaction $\text{Fe} + \text{H}_2\text{O} \rightarrow \text{FeO} + \text{H}_2$ goes to completion. Other entries in Table 1 are discussed as they arise.

Evidence has recently emerged that Earth's molybdenum—another siderophile element but somewhat less so than the HSEs—has an isotopic composition distinct from Earth's HSEs (Budde et al. 2019). This has been interpreted by its discoverers to mean that Theia—the name widely given to the Moon-forming impactor—was made of different stuff than the late veneer (Budde et al. 2019). Budde et al. (2019) even suggest that Theia was the source of Earth's water; although in our opinion, it seems equally plausible that Earth's distinctive Mo predates the Moon-forming impact. From our perspective here, it makes little difference whether Earth's water was delivered by Theia or predated Theia, because in either case, the water was present on Earth when the late veneer came.

3. Thermochemical Model

The redox state of gases in equilibrium with rocks is often described by mineral buffers that govern the capacity of the rock to consume or release oxygen. Three such buffers are described in Appendix A. Mineral buffering is most likely to matter when the rock-to-atmosphere ratio is large, as it is in meteorites or for Earth-like planets considered as a whole. Mineral buffers are less obviously appropriate for describing the interaction of meteorites with oceans and atmospheres that are much bigger than the meteorite (Elkins-Tanton & Seager 2008). Only the very biggest post-Moon-forming impacts are big enough for a mineral buffer set by the impactor to apply on a global scale. For anything smaller, the oxygen in the atmosphere and ocean much exceeds the reducing power in the impactor, and hence, the reduced mineral buffers are exhausted before the atmosphere and ocean can fully equilibrate (Elkins-Tanton & Seager 2008; Schaefer & Fegley 2017). What this means is that, in most cases, a better approximation than hewing to a mineral buffer is to stoichiometrically remove the oxygen scavenged by metallic iron from the atmosphere and ocean and then compute the resulting equilibria among the gases.

3.1. Equilibrium Chemistry

We solve for five potentially major gases—H₂, H₂O, CO, CO₂, and CH₄—while presuming that other gases are minor. In particular, we treat nitrogen as a minor perturbation, and we ignore sulfur and chlorine. We treat the equilibrium chemistry of the atmosphere as a whole. We solve for the column number densities N_j and for the partial pressures p_j of the five species. The total pressure p is the weight of the atmosphere,

$$p = g \sum_j N_j m_j, \quad (1)$$

Table 1
Some Representative Hadean Impacts

Category	N^b	M_i^c (g)	Vap ^d	Red ^e	CO ₂ ^f	Products, Dry Atmosphere ^a (bar)				
						H ₂	CO	CO ₂	CH ₄	NH ₃
Max HSE	0–1	2(25)	200	2	100	57	5(–6)	1.4(–5)	9.0	0.08
QFI ^g					100	74	1(–5)	2(–6)	7.6	0.050
IW ^g					100	35	4(–5)	6(–4)	13.7	0.086
QFM ^g					100	10	0.11	65.6	13.6	0.01
Pretty Big ^h	0–2	2.5(24)	20	0.2	20	7.6	5(–4)	0.06	2.9	0.03
					5	7.4	6(–6)	4(–4)	0.34	0.01
“Ceres”	1–4	1(24)	8	0.08	5	3.9	3(–4)	0.06	0.52	0.006
“Vesta”	2–10	2.5(23)	2	0.02	5	3.9	0.06	1.6	0.17	0.002
					2	2.6	6(–4)	0.4	0.054	0.001 5
					1	2.0	2(–4)	0.14	0.023	0.001 1
QFM ⁱ					2	1.8	1(–5)	0.02	0.28	0.06
Sub-Vesta	3–20	1(23)	0.8	0.008	5	2.7	0.005	2.7	0.008	8(–4)
QFM ⁱ					2	1.5	6(–5)	0.1	0.36	0.037
S.Pole-Ait. ^j	10–100	1(22)	0.1	8(–4)	2	0.37	0.008	1.5	1(–7)	2(–5)
QFM ⁱ					2	0.65	0.015	1.32	1(–6)	7(–5)

Notes.

^a The dry atmosphere presumes that all water has condensed at the surface.

^b Number of Hadean impacts in each class, bracketed between minimum and maximum veneer.

^c M_i presumes 33% metallic iron, like EH (high iron enstatite) chondrites or bulk Earth.

^d Oceans of water that could be vaporized by the impact.

^e Potential reducing power of the impact, expressed as oceans of water that can be reduced to H₂.

^f Atmospheric CO₂ before the impact (100 bar = 2300 moles cm⁻²).

^g Assumed to equilibrate with the named mineral buffer (defined in Appendix A).

^h Plausible size of biggest impact in a minimum late veneer.

ⁱ Atmosphere and ocean are assumed to equilibrate with QFM buffer at 650 K.

^j South Pole–Aitken is the largest impact basin preserved on the Moon.

where g is the gravity and m_j is the mass of species j . Partial pressures p_j are related to column densities and the total pressure by

$$p_j = \frac{pN_j}{\sum_j N_j}. \quad (2)$$

Note that, in general, $p_j \neq N_j m_j g$; i.e., partial pressures are proportional to number fractions, not mass fractions.

In the five gas system, hydrogen and carbon are conserved:

$$N_H = 2N_{H_2} + 2N_{H_2O} + 4N_{CH_4} \quad (3)$$

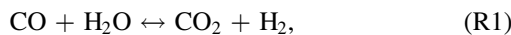
and

$$N_C = N_{CO} + N_{CO_2} + N_{CH_4}. \quad (4)$$

In the absence of a mineral buffer, oxygen is also conserved,

$$N_O = N_{H_2O} + N_{CO} + 2N_{CO_2}. \quad (5)$$

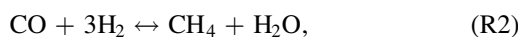
The other two relations needed to close the system are chemical equilibria. We use the water gas shift reaction



which has equilibrium constant

$$K_{R1} = \frac{p_{H_2O} p_{CO}}{p_{H_2} p_{CO_2}} \approx 18.28 \exp(-2375.6/T - 5.69 \times 10^5/T), \quad (6)$$

and the corresponding reaction for methane,



which has equilibrium constant

$$K_{R2} = \frac{p_{CH_4} p_{H_2O}}{p_{CO} p_{H_2}^3} \approx 5.239 \times 10^{-14} \exp(27285/T) \text{ atm}^{-2}. \quad (7)$$

As is customary, partial pressures in Equations (6) and (7) are in atmospheres. Equilibrium constants given here are low-order curve fits (Zahnle & Marley 2014) generated using thermochemical data from Chase (1998).

When oxygen is controlled by a mineral buffer, oxygen is not conserved, and a third chemical equilibrium reaction is needed to link the system to the mineral buffer. The mineral buffer supplies the oxygen fugacity f_{O_2} , which has units of pressure. We use



with equilibrium constant

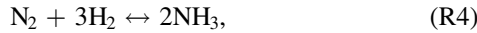
$$K_{R3} = \frac{p_{H_2O}^2}{p_{H_2}^2 f_{O_2}} \approx 1.158 \times 10^{-6} \exp(59911/T) \text{ atm}^{-1}. \quad (8)$$

We will suppose that the gas remains equilibrated with the mineral buffer until the metallic iron is either exhausted or physically removed from interaction with the gas. This fixes the total oxygen content of the atmosphere. Thereafter, the gas-phase chemistry continues to evolve with oxygen conserved in response to further cooling until the gas-phase reactions themselves quench.

It is convenient to treat nitrogen species as minor perturbations, solved separately for fixed amounts of the five important CHO species. Separating N also facilitates taking into account that nitrogen species quench at higher temperatures than H, C, and O. This simplification is accurate provided that NH_3 is not a major gas. Nitrogen is conserved,

$$N_{\text{N}} = N_{\text{NH}_3} + N_{\text{HCN}} + 2N_{\text{N}_2}. \quad (9)$$

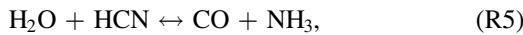
Two chemical equilibria are needed, one for ammonia



with equilibrium constant

$$K_{\text{R4}} = \frac{P_{\text{NH}_3}^2}{P_{\text{N}_2} P_{\text{H}_2}^3} \approx 5.90 \times 10^{-13} \exp(13207/T) \text{ atm}^{-2}, \quad (10)$$

and another for HCN,



with equilibrium constant

$$K_{\text{R5}} = \frac{P_{\text{H}_2\text{O}} P_{\text{HCN}}}{P_{\text{CO}} P_{\text{NH}_3}} \approx 1.99 \exp(-6339.4/T). \quad (11)$$

Equations (10) and (11) reduce to a quadratic equation for NH_3 . In practice, HCN is never produced abundantly by shock heating in the large impacts and $\text{H}_2\text{O}-\text{CO}_2$ atmospheres considered in this study. The chief source of HCN in this study is photochemical, discussed in Section 4 below.

3.2. Quenching

Chemical reactions are generally fast at high temperatures, and chemical equilibria are quickly established between major species. As the gas cools, chemical reactions between the more stable molecules slow down until, for all practical purposes, they stop, and the gas composition is said to have quenched or frozen (Zel'dovich & Raizer 1967). Here, we ignore possible catalysts and address only gas-phase chemistry, which is the most pessimistic case for methane and ammonia. We employ two quench points, one for the $\text{H}_2-\text{H}_2\text{O}-\text{CH}_4-\text{CO}-\text{CO}_2$ system and a significantly hotter one for the $\text{H}_2-\text{N}_2-\text{NH}_3-\text{HCN}$ system.

We have characterized quench conditions for CO hydrogenation to CH_4 and for N_2 hydrogenation to NH_3 in brown-dwarf atmospheres Zahnle & Marley (2014). There, we devised curve fits to global quench temperatures for the key chemical systems using a time-stepping thermochemical kinetics code employing nearly 100 chemical species and more than 1000 chemical reactions. Our curve fits are degenerate between total pressure and the H_2 partial pressure, because these are the same in brown dwarfs. For making CH_4 , our model predicts that quenching is linear with p at low pressures but quadratic with p at high pressures. The low-pressure quench temperature is

$$T_{q1}(\text{CH}_4) = \frac{42,000 \text{ K}}{\ln(3.3 \times 10^5 t_c p)}.$$

The timescale t_c is in seconds. The high-pressure form is

$$T_{q2}(\text{CH}_4) = \frac{25,000 \text{ K}}{\ln(0.025 t_c p^2)}.$$

The quench temperature is the smaller of the two,

$$T_q(\text{CH}_4) = \min(T_{q1}(\text{CH}_4), T_{q2}(\text{CH}_4)). \quad (12)$$

Other published estimates of quench conditions in the $\text{CH}_4-\text{CO}-\text{H}_2$ system (see Prinn & Barshay 1977; Line et al. 2011; Visscher & Moses 2011) are similar enough that they also predict CH_4 -dominated atmospheres for the cases where we predict them; the different chemical quenching times are explicitly compared in Zahnle & Marley (2014).

Quenching in the NH_3-N_2 system occurs at higher temperatures,

$$T_q(\text{NH}_3) = \frac{52,000 \text{ K}}{\ln(1.0 \times 10^7 t_c p)}. \quad (13)$$

Typically $T_q(\text{NH}_3)$ is about 300 K warmer than $T_q(\text{CH}_4)$. There is considerable uncertainty regarding the mechanisms of N_2 hydrogenation, with resulting considerable uncertainty in quenching times. The older estimate by Prinn & Fegley (1981) predicts slower chemistry, while two more recent estimates (Line et al. 2011; Zahnle & Marley 2014) give similar results for conditions encountered here. In practice, the different kinetics predict similar chemical compositions (Zahnle & Marley 2014), because the NH_3/N_2 ratio is not strongly sensitive to temperature. Figure 1 illustrates quenching after a Vesta-scale impact.

3.3. Cooling Times

Impacts that vaporize the oceans create globally hot, high-pressure conditions that can last for thousands of years. The energy invested in evaporating water and heating the major atmospheric gases in an ocean-vaporizing impact is

$$E_{\text{atm}} = (Q_w + C_{\text{H}_2\text{O}} \Delta T) M_{\text{H}_2\text{O}} + C_{\text{CO}_2} \Delta T M_{\text{CO}_2} + C_{\text{N}_2} \Delta T M_{\text{N}_2} \quad (14)$$

where $C_{\text{H}_2\text{O}} = 2 \times 10^7 \text{ erg g}^{-1} \text{ K}^{-1}$, $C_{\text{CO}_2} = 8 \times 10^6 \text{ erg g}^{-1} \text{ K}^{-1}$, and $C_{\text{N}_2} = 1.1 \times 10^7 \text{ erg g}^{-1} \text{ K}^{-1}$ are heat capacities of H_2O , CO_2 , and N_2 , respectively; $Q_w = 2.5 \times 10^{10} \text{ erg g}^{-1}$ is the latent heat of vaporization of H_2O at 273 K; and $\Delta T \sim 1500 \text{ K}$ approximates heating the atmosphere to a point where rock vapors become significant. Evaluated for relevant parameters,

$$E_{\text{atm}}(\text{erg}) = 8 \times 10^{34} \left(\frac{M_{\text{H}_2\text{O}}}{1.4 \times 10^{24} \text{ g}} \right) + 6 \times 10^{33} \left(\frac{M_{\text{CO}_2}}{5 \times 10^{23} \text{ g}} \right) + 8 \times 10^{31} \left(\frac{M_{\text{N}_2}}{5 \times 10^{21} \text{ g}} \right) \quad (15)$$

where the fiducial masses correspond to an ocean of water, a 100 bar CO_2 atmosphere, and a 1 bar N_2 atmosphere, respectively.

Evaporating the oceans and heating the steam to the temperature of the condensing rock vapor are the big terms in the energy budget for impacts of this scale. This energy is

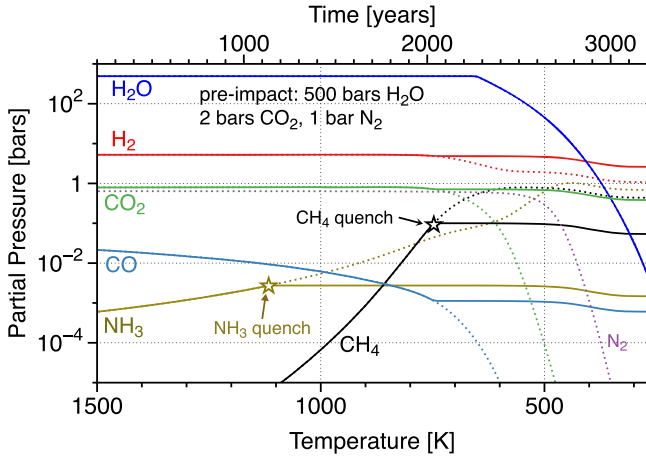


Figure 1. Example of quenching after a Vesta-sized impact into an Earth with a pre-impact atmosphere containing 2 bar CO_2 , 1 bar of N_2 , and 1.85 oceans (500 bar) of liquid water. Cooling (time) marches monotonically from left to right. Quench points for CH_4 and NH_3 H_2 - N_2 - NH_3 are indicated with stars. Solid lines show quenched compositions while dotted lines extend the equilibria to temperatures colder than the quench point for gas-phase reactions. Partial pressures are also affected by water condensation ($T < 650$ K).

compared to the impact energy

$$E_i(\text{erg}) = \frac{1}{2} m_i v_i^2 = 1.5 \times 10^{35} \left(\frac{m_i}{10^{23} \text{ g}} \right) \left(\frac{v_i}{17 \text{ km s}^{-1}} \right)^2. \quad (16)$$

If half of the impact energy is spent heating and vaporizing water (with the other half deeply buried and unavailable on timescales shorter than thousands of years, or promptly radiated to space at higher temperatures in the immediate aftermath of the event), a Vesta-size impact can evaporate and heat 2.3 oceans of water. The maximum HSE impact exceeds the Vesta-size impact by a factor of 100. Put another way, an EH-like (high iron, enstatite chondritic) impact creates 100 times more steam than hydrogen.

The characteristic cooling time t_c is approximated by how long it takes for the steam atmosphere to cool to the quench point. Quench temperatures for methane and ammonia will be hotter than water's critical point, so we ignore the latent heat released by condensation.

$$t_c = \frac{C_{\text{H}_2\text{O}} \times M_{\text{H}_2\text{O}} + C_{\text{CO}_2} \times M_{\text{CO}_2} + C_{\text{N}_2} \times M_{\text{N}_2}}{A_{\oplus} F_{ir}} \times (T - T_q), \quad (17)$$

where A_{\oplus} is the area of the Earth, and $F_{ir} \approx 1.5 \times 10^5 \text{ erg cm}^{-2} \text{ s}^{-1}$ is the radiative cooling rate of a terrestrial steam atmosphere with a 50% albedo after the Sun has reached the main sequence (ca. 50 Myr). This cooling rate is valid provided that water clouds condense somewhere in the atmosphere (Abe & Matsui 1988; Nakajima et al. 1992). For methane, for which quench temperatures are of order 800 K, the relevant cooling is from 1400 to 800 K. Evaluated,

$$t_c(\text{s}) = 2 \times 10^{10} \left(\frac{M_{\text{H}_2\text{O}}}{1.4 \times 10^{24} \text{ g}} \right) + 3 \times 10^9 \left(\frac{M_{\text{CO}_2}}{5 \times 10^{23} \text{ g}} \right) + 4 \times 10^7 \left(\frac{M_{\text{N}_2}}{5 \times 10^{21} \text{ g}} \right), \quad (18)$$

which is of the order of 1000 yr for most cases we consider. For NH_3 , whose quench temperature is ~ 300 K hotter than methane's, the cooling time is about half as long.

If an impact is too small to fully vaporize the ocean, the ocean remains cool and acts as a heat sink that competes with thermal radiation to space. In the relevant case, the impact leaves the atmosphere much hotter than the ocean and mostly made of H_2 and water vapor. The lower atmosphere will therefore be stable against convection. Under these conditions, the flow of energy down to the ocean is limited by radiative transfer. To illustrate, compare the diffusive flux of downward radiation in the Eddington approximation (any astronomy textbook),

$$F_{\downarrow} = \frac{16}{3} \frac{\sigma_B T^3}{\kappa \rho} \frac{dT}{dz}, \quad (19)$$

to Earth's net cooling rate F_{ir} . The gray approximation opacity of water vapor is $\kappa \approx 0.1 \text{ cm}^2 \text{ g}^{-1}$ (Nakajima et al. 1992). Assume 30 bar of 1100 K steam as an example, for which the density at the surface is $\rho = 0.025 \text{ g cm}^{-3}$ and the surface temperature is 500 K (both set by the boiling point). The temperature gradient appropriate to cooling the whole atmosphere is 600 (=1100–500) K over a 20 km scale height. With $dT/dz = 3 \times 10^{-4} \text{ K cm}^{-1}$, we estimate that $F_{\downarrow} \approx 0.5 \times 10^5 \text{ erg cm}^{-2} \text{ s}^{-1}$, which is 30% of net cooling (F_{ir}) to space. The radiative flux F_{\downarrow} is relatively small because $\rho \kappa$ is big. (In this example, F_{\downarrow} would exceed F_{ir} for impacts that generate less than 10 bar of steam.) We conclude that, in general, relatively little of the energy in a hot deep steam atmosphere will flow downward to the ocean. The chief exception would be if there is enough CO_2 that the much hotter atmosphere is nonetheless dense enough to sink in cooler steam. This might happen for smaller impacts in deep CO_2 atmospheres, and if it did, it would result in complications that we will not address here.

3.4. Results

We consider three classes of impact.

(i) If the impact is big enough, it delivers enough iron to fully reduce all of the H_2O and CO_2 at the surface. Under these conditions, the $\text{Fe} + \text{H}_2\text{O} \leftrightarrow \text{FeO} + \text{H}_2$ equilibrium is likely to govern the oxidation state of the atmosphere throughout the cooling phase. Earth's maximum HSE impact was in this size range. The iron-wüstite (IW) buffer describes the simple reaction of iron and steam to make FeO (wüstite) and H_2 , and so it is likely to be kinetically favored in the short term. On longer timescales, the more reducing quartz-fayalite-iron buffer (QFI, effectively a buffer between iron and olivine) may dominate. Both mineral buffers favor CH_4 , but the QFI buffer would also consume most of the H_2O in favor of H_2 . The latter outcome resembles the story proposed to explain the desiccation of Mars by Dreibus et al. (1989) and Kuramoto (1997).

A caveat is that, for impacts of this scale, the global ejecta blanket should have been tens of kilometers thick. Although the molten iron in the ejecta must have passed through the atmosphere and ocean to reach the surface—Genda et al. (2017b) estimate that more than half the iron is initially disseminated as mm-sized droplets—it is plausible that some of the iron was buried before it could react with H_2O or CO_2 . If so, some of the reducing power of the impact would at first have been sequestered from the surface, only becoming

available as reduced gases emitted to the atmosphere on a longer geologic timescale. Modeling the fate of iron in the post-impact mantle is beyond the scope of this study.

(ii) The oceans are fully vaporized but there is not enough metallic iron in the impact to reduce all of the H_2O in the ocean to H_2 . Impacts on this scale leave much of the H_2O and CO_2 unreacted. In such an impact, the ejecta blanket is not much thicker than the ocean is deep, and conditions at the surface are supercritical for water, promoting efficient chemical coupling of the water with the iron while the iron lasts (see Choudhry et al. 2014, and references therein). There are of the order of 10 such impacts in a representative maximum late veneer, and 1–3 in a minimum late veneer. We assume that in these events, the introduced Fe consumes oxygen from the water and CO_2 until all of the injected Fe is gone. Thereafter, the atmosphere evolves with its oxygen content (in H_2O , CO , and CO_2) held constant. In these events, the steam atmosphere is deep, thick, and hot, and cooling is slow, conditions that strongly favor CH_4 and, to a lesser degree, NH_3 .

(iii) The impact is too small to fully vaporize the oceans. These events feature faster cooling times and lower atmospheric pressures, with the amount of steam generated proportional to the energy released by the impact. The lower pressures are generally much less favorable to CH_4 formation, but small impacts are interesting because there are more of them and they are likelier to be survived by life or its precursors. For small impacts, we will find that the QFM mineral buffer often generates a more reduced gas composition than predicted from scavenging by impact iron of the oxygen in the hydrosphere and atmosphere. For these events, we will presume that the ferrous iron already present in the crust is available as an additional sink of oxygen at the QFM buffer. These matters are discussed in more detail below.

We treat the volume of the ocean and the amount and state of carbon in the atmosphere before the impact as initial conditions. For water, we assume that 1.85 oceans of water (5 km) were present at the surface. Bigger oceans allow for more extensive loss of hydrogen to space without desiccating the planet. We take the view, provisionally, that a much drier planet ($\ll 1$ ocean) will not evolve to Earth as we know it.

Carbon reservoirs are not well constrained. Between surface, crust, and mantle, Earth may hold the equivalent of 200 ± 100 bar of CO_2 (Sleep & Zahnle 2001; Dauphas & Morbidelli 2014). One end-member is hot and oxidized, with CO_2 being initially divided roughly equally between a melted QFM mantle and Henry Law partitioning of 100 bar of CO_2 in the atmosphere in the aftermath of the Moon-forming impact (Holland 1984; Abe 1997; Zahnle et al. 2007; Elkins-Tanton 2008). An oxidized mantle could have been consequent to a previous history of hydrogen escape or to iron-mineral disproportionation (Frost & McCammon 2008). CO_2 can also be generated from thermal decomposition of carbonate minerals if these were near the surface. Although we do not explicitly consider more reduced atmospheres (CO or CH_4) as initial conditions, we will find below that thick CO or CH_4 atmospheres can be long-lasting in the Hadean. The CO_2 atmosphere is the most oxidized and, hence, the most conservative case. We treat p_{CO_2} as a free parameter.

Table 1 lists a sampling of possible Hadean impacts. Before impact, Earth is presumed to have had 1.85 oceans of water at the surface (500 bar, $28.3 \text{ kmols cm}^{-2}$) and one bar (36 moles cm^{-2}) of N_2 in the atmosphere. The amount of

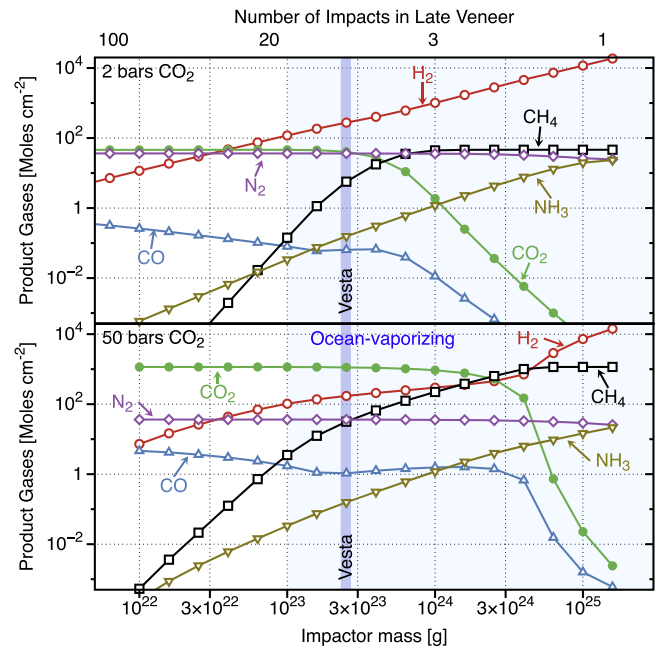


Figure 2. Quenched impact-induced transient atmospheres as a function of impactor mass (EH composition) for two pre-impact atmospheres, one with 50 bar of CO_2 and the other with 2 bar. Both have 1 bar of N_2 and 1.85 oceans (500 bar) of water on the surface. Inventories are shown in moles to highlight the chemical transformation. A Vesta-size impact is indicated by the shaded vertical bar. Potentially ocean-vaporizing impacts are indicated by lighter shading. A rough guide to the number of impacts of a given size is listed across the top. In these models, all reducing power is furnished by the quantitative reduction of the impactor’s Fe to FeO; no mineral buffering is assumed. In the maximum late veneer impact (at right), nearly all CO and CO_2 are converted to CH_4 .

CO_2 varies between examples. “100 bar” of CO_2 corresponds to $2300 \text{ moles cm}^{-2}$.

Figures 2 and 3 show post-impact atmospheres for a wide range of impact sizes for 2 and 50 bar of CO_2 . Figure 2 shows column densities (moles cm^{-2}), which makes the chemical trends clear, while Figure 3 shows the same information as partial pressures. The reducing power of the impactors presumes high iron EH (enstatite) or H (ordinary) chondritic bodies (33% Fe by mass, which also approximates the bulk Earth). Impact energy assumes an impact velocity of 17 km s^{-1} . Table 1 lists major product gases for each case. Many of the cases listed in the table are used as initial conditions for photochemical evolution in Section 3 below. If the Fe is incompletely used up, the corresponding impact mass can simply be scaled up; i.e., if half the Fe goes unreacted, the required impactor would have twice the mass.

The maximum HSE impact delivers marginally enough Fe to fully reduce the atmosphere and hydrosphere, which suggests that equilibration with a mineral buffer may be plausible. Table 1 lists several maximum HSE cases with 100 bar of CO_2 equilibrated to different buffers. The QFI buffer, which would also fully reduce the atmosphere and hydrosphere, seems likeliest if the reactions all go to completion. But if much of the iron is buried before it reacts, a more oxidized buffer might be more reasonable.

In the next category, the “Pretty Big” cases approximate the biggest impact in our lower bound late veneer, while “Ceres” and “Vesta” are impacts with the mass of the real Ceres and the real Vesta. These are all ocean-vaporizers, but none deliver nearly enough iron to fully reduce the ocean. Figure 4

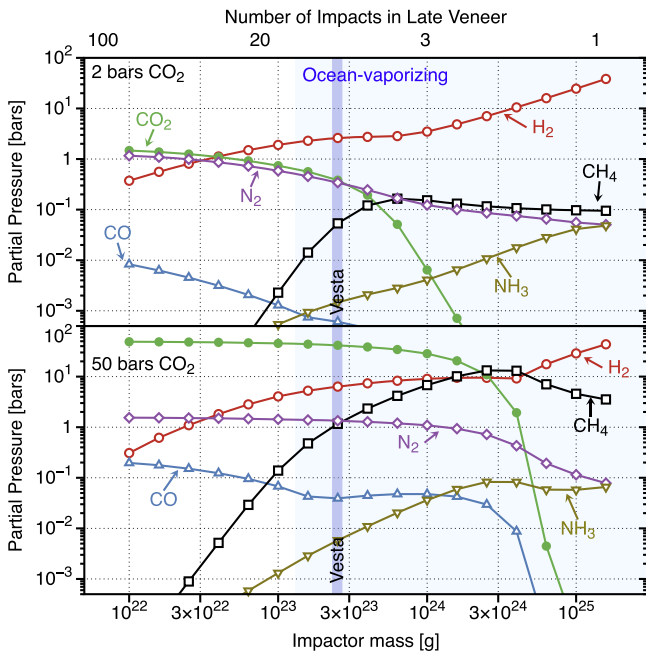


Figure 3. Same as Figure 2 but atmospheric compositions are shown as partial pressures.

compares outcomes as a function of $p\text{CO}_2$ for Ceres-sized impacts.

The third category is represented in Table 1 by two “sub-Vestas” and the lunar South Pole–Aitken impact that do not fully evaporate the oceans. These are small enough that life or its precursors might survive. These impacts are also too small to deliver enough metallic iron to reduce the ocean to the QFM composition. This means that the reducing power of Earth’s mineral buffers—made active by the heat of the impact—needs to be taken into account. The South Pole–Aitken basin is an example of a relatively minor event.

Table 1 lists two sub-Vestas. The first uses only the reducing power of the impact. This is the most pessimistic case. The other assumes equilibration with a crustal QFM mineral buffer, but at an arbitrary lower quench temperature of 650 K. In effect, the second case asks what happens if supercritical water was in itself enough to ensure that the coupled $\text{H}_2\text{--H}_2\text{O--CO--CO}_2\text{--CH}_4\text{--N}_2\text{--NH}_3$ system equilibrated on a 1000-yr timescale. This can be viewed as the optimistic limit on what sub-ocean-vaporizing impacts can do to generate species like CH_4 and NH_3 .

Figure 5 illustrates the potential inherent in the more optimistic case. Here, we assume that the atmosphere and ocean remain chemically equilibrated with the crust or mantle at the QFM buffer while water remains supercritical; i.e., we set $T_q = 650$ K. The QFM buffer is only weakly reducing because it has only Fe^{+2} to offer as a reductant. On the other hand, there is a great deal of Fe^{+2} available in impact-heated crust and mantle materials, although the crustal source is not inexhaustible.

To illustrate these considerations, in Figure 5, we estimate the depth in the crust (global average) to which FeO must be oxidized to Fe_3O_4 (magnetite), assuming that the crust was 10% FeO by mass and that all of the FeO is oxidized to Fe_3O_4 , and taking into account the reducing power delivered by the impact as metallic iron. Figure 5 presumes a pre-existing atmosphere with the equivalent of 2 bar of CO_2 and one bar of N_2 . The figure shows that, even in a Vesta-scale impact, the

required reducing power can be extracted from FeO in the uppermost 3 km of a QFM crust. Smaller impacts use less of Earth’s FeO because they do not evaporate the entire ocean, while larger impacts (larger than 4×10^{23} g in Figure 5) deliver more metallic iron than needed to maintain QFM.

4. Photochemical Evolution of Impact-generated Transient Atmospheres

Our goal in this section is to model the photochemical decay of the impact-generated transient reduced atmosphere. In particular, we are interested in what happens to methane. The key processes driving the atmosphere’s evolution are ultraviolet photolysis and hydrogen escape. Thus, fundamentally, we are most concerned with counting the photons and apportioning their effects.

4.1. The Photochemical Model

In the photochemical model, we consider six major species: H_2 , CH_4 , H_2O , CO_2 , CO , and N_2 . Minor species include HCN (nitriles), C_2H_n (a mix of C_2H_2 , C_2H_4 , C_2H_6), and organic haze. Other molecules and free radicals that are considered include NO , NH , $\text{N}(^4\text{S})$, $\text{N}(^2\text{D})$, $\text{O}(^3\text{P})$, $\text{O}(^1\text{D})$, $^3\text{CH}_2$, $^1\text{CH}_2$, CH_3 , and OH . We refer to ground-state $\text{N}(^4\text{S})$ as N, ground-state $\text{O}(^3\text{P})$ as O, and ground-state $^3\text{CH}_2$ as CH_2 . Key reactions are listed in Appendix B. Atomic H is implicit and lumped with H_2 for accounting purposes. Ions are not explicitly included, although the first-order effects of ion chemistry are taken into account as loss processes for CO_2 and CH_4 (Appendix C).

Our purpose is to construct the simplest model that captures the first-order consequences of photochemical evolution of unfamiliar atmospheres, while conserving elements and counting the photons. Anything more complicated (e.g., a 1D atmospheric photochemistry code) would necessarily introduce several poorly constrained free parameters. We therefore assume that the major atmospheric constituents are uniformly distributed vertically, affected only by the totality of chemical and physical sources and sinks. We treat each major species j as a column density N_j (units of number per cm^2). Ultraviolet photons are sorted into several spectral windows, and the effects of photolysis are apportioned in accordance with the first-order consequences of photochemistry; these simplifications will be discussed in detail below. The columns are evolved through time by integrating dN_j/dt . Hydrogen escape and the effectively irreversible photolysis of methane impose direction.

There are two first-order complications to the simplest model that demand attention. First, H_2O —usually the most abundant gas after the impact—condenses to make oceans. Thereafter, its abundance at stratospheric altitudes where photolysis takes place is limited by the atmosphere’s cold trap. Water vapor is key to these models because water vapor is often the major oxidant. The drier the stratosphere, the more slowly it evolves and the more likely it is to favor reduced products like hydrocarbons. A next-generation study might investigate the water vapor contents of self-consistent radiative-convective atmospheres, but this level of modeling goes beyond the scope of this study. Here, we treat stratospheric water vapor in the atmosphere as a free parameter.

The second complication is the shadow cast by organic hazes. Organic hazes are expected when methane is abundant and subject to UV photolysis (Trainer et al. 2006; Hörst et al. 2012, 2018). The analogy is Titan. We expect Earth’s hazes, when present, to be optically thick, much thicker than on Titan

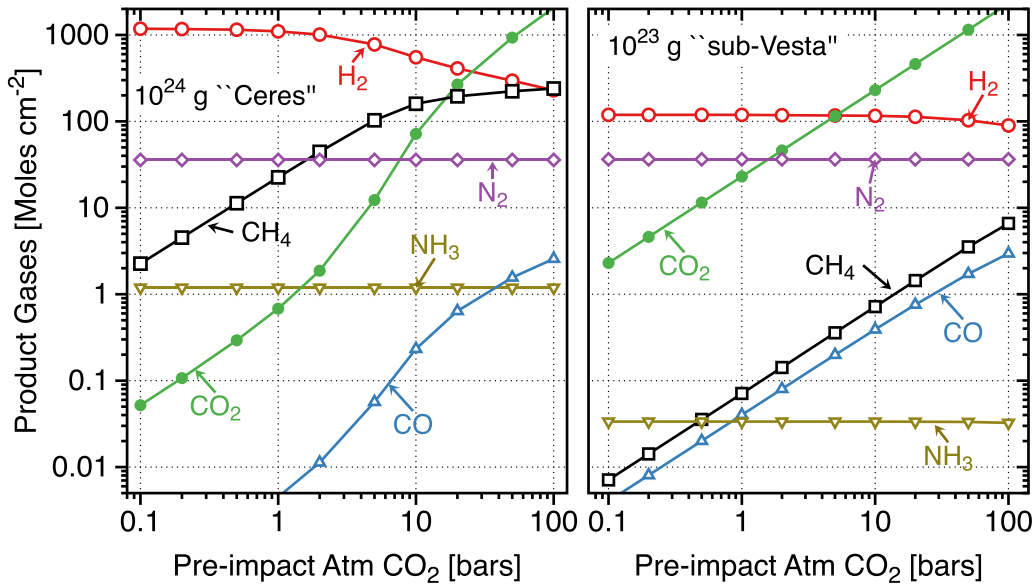


Figure 4. Quenched impact-induced transient atmospheres as a function of how much CO₂ was in the atmosphere before the impact, for two sizes of impact, one ocean-vaporizing and one not. The pre-impact Earth has 1 bar of N₂ and 1.85 oceans (500 bar) of water on the surface. The Ceres-sized (10²⁴ g) impact (EH) is big enough to convert thinner CO₂ atmospheres to CH₄, but it does not have enough Fe to fully reduce the thicker CO₂ atmospheres. The smaller “sub-Vesta” impact is too small to fully vaporize 1.85 oceans; the chief effect is to make a lot of H₂.

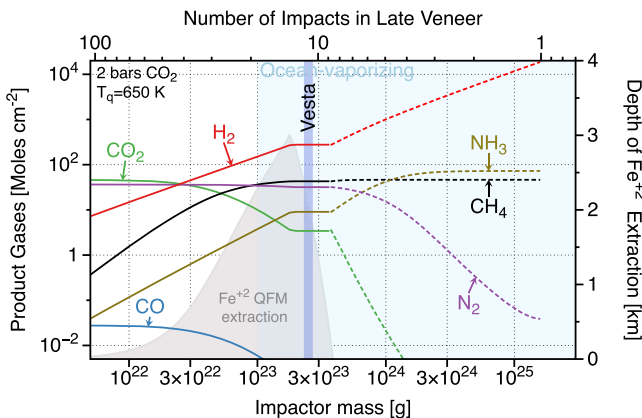


Figure 5. The left-hand axis shows gas compositions as a function of impact mass when quenching is assumed to take place at 650 K (water’s critical temperature). Solid lines for smaller impacts ($M_i < 4 \times 10^{23}$ g) show gas compositions in equilibrium with the QFM mineral buffer. The right-hand axis shows the depth (shading) to which FeO in the crust must be oxidized to magnetite (Fe₃O₄) to maintain equilibrium with the QFM buffer at 650 K. Dashed lines for gas compositions generated by bigger impacts ($M_i > 4 \times 10^{23}$ g) are determined by metallic iron delivered by the impact. These latter compositions are no more reduced than the otherwise comparable compositions seen for gas-phase quenching in Figure 2 above, but the assumed low 650 K quench temperature favors CH₄ and NH₃ over H₂.

today, because UV irradiation of early Earth was at least 1000 times greater than of modern Titan. Here, we follow Wolf & Toon (2010) and parameterize haze optical depth as a function of haze production rate. Because water photolysis would be the major source of oxidants in a methane-rich atmosphere, the competition between hazes and water for UV photons creates a positive feedback in which one or the other dominates.

4.1.1. Irradiation

We divide the solar FUV and EUV spectrum into six windows that align with particular properties of the atmosphere

(Table 2). We neglect the Lyman continuum (80–91.2 nm, current photon flux of 8×10^9 cm⁻² s⁻¹) as filtered out by atomic H. Absorption at wavelengths longer than the Lyman continuum usually leads to dissociation of molecules into two neutral species. Absorption at wavelengths shorter than the Lyman continuum usually ionizes the molecule, leaving the molecule provisionally intact as an ion.

The ancient Sun was a stronger source of EUV radiation than is the modern Sun. We scale the different channels according to the general rule that hotter source regions are relatively more enhanced by solar activity and were therefore relatively more enhanced when the Sun was young (Zahnle & Walker 1982; Claire et al. 2012). Enhancement factors for the different windows are listed in Table 2.

Total column photolysis rates Φ_j (cm⁻² s⁻¹) for species j allow for competition for photons between species,

$$\Phi_j = \frac{1}{4} \sum_{i=2,6} F_i S_i \frac{\sigma_{ij} N_j}{\sum_{k=1,7} \sigma_{ik} N_k}, \quad (20)$$

where k is an index running over the species. This approach conserves photons, which is the principal requirement here. Photoionization is treated separately,

$$\Phi_j^* = \frac{1}{4} F_1 S_1 \frac{\sigma_{1j} N_j}{\sum_k \sigma_{1k} N_k}. \quad (21)$$

Organic hazes, when present, may provide UV protection to the deeper atmosphere (Sagan & Chyba 1997; Pavlov et al. 2001; Wolf & Toon 2010). Wolf & Toon (2010) constructed a microphysical model of organic hazes of early Earth. They considered spherical haze particles and “fractal” haze particles, with the latter model much preferred by its authors. We fit power laws to the fractal haze optical depths listed in their Table S1 as a function of the haze production rate,

$$\tau_{uv} \approx 10 \left(\frac{dN_{haze}/dt}{3 \times 10^{10}} \right)^{0.8} \quad (22)$$

Table 2
Fluxes ($\text{cm}^{-2} \text{s}^{-1}$) and Cross Sections (cm^2)

	Spectral Window					
	EUV ₁ ^a	EUV ₂ ^b	EUV-N ₂ ^c	Ly α	FUV-CO ₂	FUV-H ₂ O
<i>i</i>	1	2	3	4	5	6
λ (nm)	<80	91.2–117	91–100	121.5	125–170	170–185
F_{λ} ^d	3×10^{10}	2×10^{10}	3.6×10^9	3.6×10^{11}	4×10^{11}	2.5×10^{12}
S_{λ} ^e	30	20	10	10	7	4
<i>j</i>	Cross section σ_{ij} (cm^2)					
1	H ₂	2×10^{-18}	2×10^{-18}
2	CH ₄	2×10^{-17}	8×10^{-18}	8×10^{-18}	8×10^{-18}	...
3	H ₂ O	1.3×10^{-17}	8×10^{-18}	8×10^{-18}	8×10^{-18}	1×10^{-18}
4	CO ₂	2×10^{-17}	4×10^{-17}	4×10^{-17}	5×10^{-20}	8×10^{-19}
5	CO	1.3×10^{-17}
6	N ₂	1.3×10^{-17}	...	2.5×10^{-16}

Notes.

^a Photoionizing EUV excluding the Lyman continuum.

^b EUV₂ excludes photoionizing radiation and radiation that photolyzes N₂.

^c EUV-N₂ is the portion of non-photoionizing EUV that coincides with N₂ absorption.

^d Quiet Sun irradiance, photons $\text{cm}^{-2} \text{s}^{-1}$ at 1 au.

^e Young Sun enhancement over modern quiet Sun.

and

$$\tau_{\text{vis}} \approx 0.5 \left(\frac{dN_{\text{haze}}/dt}{3 \times 10^{10}} \right)^{0.7}. \quad (23)$$

The ultraviolet optical depth refers to 197 nm, and the visible optical depth refers to 564 nm. We have converted units from production in grams per year to the equivalent number of carbon atoms $\text{cm}^{-2} \text{s}^{-1}$, which are the units used in this paper. Haze production rates on early Earth can exceed 1×10^{12} carbon atoms $\text{cm}^{-2} \text{s}^{-1}$, which corresponds to UV and visible fractal haze optical depths of the order of 160 and 6, respectively.

Hazes can suppress H₂O photolysis if the stratosphere is dry. This can lead to a positive feedback that encourages haze formation. As hazes thicken, there is less H₂O photolysis and less oxidation, which favors more haze formation. The consequence of this positive feedback resembles a phase change, in which much of the carbon derived from methane photolysis polymerizes into a wide range of heavier, generally oxygen-deficient organics (which we loosely refer to as “haze”) that precipitate to the troposphere and probably to the surface.

In wetter stratospheres, haze formation competes with oxidation consequent to H₂O photolysis. The organics and hazes that form under these conditions will contain more oxygen, suggesting a relatively greater role for acids, aldehydes, carbonyls, and other more water-soluble molecules that are more likely to rain out when they reach the troposphere. These may be essential ingredients for genesis of ribose for the RNA world (see Benner et al. 2019b).

4.1.2. Photolysis

Methane photolysis is dominated by Ly α radiation. Methane photolysis at Ly α mostly yields an excited methylene radical ¹CH₂ plus hydrogen (Huebner et al. 1992). Singlet methylene can be collisionally de-excited to the less reactive triplet ³CH₂, or it can react with CH₄ or H₂ to make CH₃ radicals. We will refer to these small radicals generically as CH_{*n*}. Both CH₂ and CH₃ react very quickly with atomic N from N₂ photolysis to

make C–N bonds or with atomic O from CO₂ photolysis to make C–O bonds. The C–O bonds once formed are difficult to break photochemically. The N reactions are the primary sources of HCN in a CH₄–N₂ irradiated atmosphere. We neglect the possible catalytic role of N₂ through the CH₂N₂ (diazomethane) intermediary.

Competition for Ly α photons is limited. We do not expect scattering by atomic hydrogen to be significant, because the solar Ly α emission is much broader than the velocity dispersion in hydrogen atoms at atmospheric temperatures. CO₂ has a very small cross section to Ly α , only about 0.5% of methane’s. Both H₂ and CO have hot absorption lines that partially overlap with Ly α emission. Resulting fluorescence has been seen in planetary nebulae (Lupu et al. 2006) and cometary comae (Lupu et al. 2007), respectively. However, the effect requires ro-vibrationally excited H₂ and CO molecules and, hence, is unlikely to be important at relevant conditions. Water’s cross section at Ly α is about the same as methane’s, but we do not expect H₂O to be abundant at the highest altitudes once the cold trap has been established in the lower atmosphere. What this all means is that, when methane is abundant, Ly α photochemistry takes place high in the atmosphere, aligning it with N₂ photolysis and generally favoring the production of organic hazes and nitriles. When methane is not abundant, Ly α photochemistry takes place deeper in the atmosphere, which better aligns methane photolysis with CO₂ photolysis and H₂O photolysis, an alignment that favors methane oxidation and disfavors nitrile production.

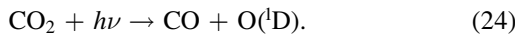
Nitrogen (N₂) photolysis is dominated by several very strong narrow absorption bands that coincide with solar emission lines. Huebner et al. (1992) stress the importance of the overlap between a strong N₂ band and solar Ly γ (92.25 nm). Comparison between the solar spectrum (Curdt et al. 2001) and the N₂ absorption spectrum predicted by Liang et al. (2007), Li et al. (2013), and Heays et al. (2014) shows that strong N₂ absorption bands coincide with several other Lyman lines, including Ly δ (94.974 nm), Ly ϵ (93.78 nm), Ly 7, 8, and 12, and also with an N III line (99.17 nm). There is also overlap at 91.3 nm where Lyman lines ($n > 30$) pile up in the approach to the Lyman limit. Huebner et al. (1992) estimated

from a suite of discordant experiments that the N_2 photolysis cross section at Ly γ is of the order of $2.5 \times 10^{-16} \text{ cm}^2$.

Nitrogen's chief competition for photons is with CO_2 , which has big cross sections of order $4 \times 10^{-17} \text{ cm}^2$ at wavelengths where N_2 absorbs. Molecular hydrogen also absorbs at some of these wavelengths, Ly γ in particular, but cross sections are generally smaller than 10^{-18} cm^2 . For the quiet Sun at Earth, we estimate a total N_2 photolysis rate of $3.6 \times 10^9 \text{ cm}^{-2} \text{ s}^{-1}$, which agrees well with what Liang et al. (2007, their Figure 2) compute for Titan when scaled to 1 au.

Photolysis between 91.2 and 100 nm splits N_2 into a ground-state N atom and an electronically excited $N(^2D)$. The $N(^2D)$ can react with H_2 or CH_4 to make NH, react with CH_4 to make CH_2NH , and react with CO_2 to make CO and NO (Herron 1999). Both NH and NO react rapidly with N to reconstitute N_2 . Otherwise, the most important N and NH reactions are with hydrocarbon radicals to make HCN and other nitriles, such as acetonitrile (CH_3CN) and cyanoacetylene (HCCCN). Photolytic production of HCN has been predicted to work well in an N_2 - CO_2 atmosphere (Zahnle 1986; Tian et al. 2011). Photochemical organics have been hypothesized as a source of reduced nitrogen and reduced carbon that can be subducted by the mantle (Wordsworth 2016).

At the top of the atmosphere, CO_2 photolysis is dominated by EUV wavelengths between 91.2 (the Lyman limit) and 115 nm. Weaker absorption at FUV wavelengths between 130 and 180 nm can be as important if other absorbers are not abundant. At FUV wavelengths, CO_2 photolysis usually creates a ground-state CO molecule and a highly reactive $O(^1D)$ atom.



At the shorter wavelengths, photolysis can also yield electronically excited CO and a ground-state O atom (Huebner et al. 1992). We will assume that excited CO is de-excited by collisions.

The $O(^1D)$ atom is highly reactive, including reaction with CH_4 to liberate CH_3 . Key $O(^1D)$ reactions are listed in Appendix B. It can be de-excited to the less reactive $O(^3P)$ ground state by collisions with CO_2 , N_2 , and CO, but it reacts quickly with CH_4 and H_2 . By contrast, reactions of ground-state O with CH_4 and H_2 are negligibly slow at 300 K. We therefore take the initial reaction of $O(^1D)$ with CH_4 as the rate-limiting step for CH_4 loss from CO_2 photolysis. Subsequent reactions of O with free radicals like CH_3 are fast and result in CO bonds.

Carbon monoxide has a similar spectrum to N_2 , but unlike N_2 , few of its bands align with strong solar emission lines. CO dissociation into neutral atoms is dominated by the Lyman continuum (Huebner et al. 1992) and, hence, is relatively unimportant in hydrogen-rich atmospheres.

Water photolysis yields OH and H for FUV with $\lambda < 190 \text{ nm}$. If the stratosphere is very dry, organic hazes have potential to shield H_2O from photolysis, especially at wavelengths $\lambda > 182 \text{ nm}$, where H_2O 's cross section starts to fall off rapidly with increasing λ .

Because we do not distinguish between H and H_2 , hydrogen photolysis is important only as opacity.

Ammonia is swiftly photolyzed by UV radiation between $185 < \lambda < 215 \text{ nm}$ at wavelengths where H_2O and CO_2 absorptions are very weak. The products are highly reactive NH and NH_2 radicals (Huebner et al. 1992). These can lead to

N_2 formation, but they can also react with hydrocarbons if the latter are plentiful.

4.1.3. The Methane Budget

Methane ends up either as organics or HCN, or is oxidized to CO or CO_2 . While CH_4 is preponderant, photochemistry following photolysis will tend to generate hydrocarbons (Lasaga et al. 1971; Yung & Pinto 1978; Zahnle 1986; Trainer et al. 2006; Hörst et al. 2018) and nitrogenous organics. When CO_2 is preponderant, methane is more often oxidized to formaldehyde (HCHO) or CO.

Methane can also be oxidatively attacked by products of H_2O photolysis and CO_2 photolysis. The most important of these are $O(^1D)$ atoms from CO_2 photolysis (R32) and OH from H_2O photolysis or reaction of $O(^1D)$ with H_2 . (Reactions of CH_4 with H and ground-state O atoms are slow unless the gas is much hotter than we have assumed, while reaction with $N(^2D)$ typically creates nitriles.) OH reacts fairly rapidly with CO to make CO_2 , and more slowly at room temperature with H_2 or CH_4 to yield H_2O . The reactions of OH with H_2 and CH_4 are sensitive to temperature, while the reaction with CO is not. At 300 K, $OH + CO \rightarrow CO_2$ is about $20\times$ faster than reaction with H_2 or CH_4 , and at 250 K, it is about $100\times$ faster.

Column oxidative loss of CH_4 is approximated by loss reactions with $O(^1D)$ from CO_2 photolysis and OH from H_2O photolysis:

$$\left(\frac{dN_{CH_4}}{dt}\right)_{ox} = -\Phi_{CO_2} \left(\frac{k_{22}N_{CH_4}}{\sum_j k_{2j}N_j}\right) - \Phi_{H_2O} \left(\frac{k_{32}N_{CH_4}}{\sum_j k_{3j}N_j}\right). \quad (25)$$

The total CH_4 budget sums the photolytic, photoionic, and oxidative losses,

$$\frac{dN_{CH_4}}{dt} = -\Phi_{CH_4} + \left(\frac{dN_{CH_4}}{dt}\right)_{ions} + \left(\frac{dN_{CH_4}}{dt}\right)_{ox}. \quad (26)$$

4.1.4. Hydrocarbons and Organic Hazes

Reactions between CH , CH_2 , and CH_3 lead to acetylene, ethylene, ethane, and eventually to more complicated hydrocarbons that can form a high-altitude haze. The chief competing reactions are those with O or OH radicals. We lump acetylene, ethylene, and ethane together as C_2H_n hydrocarbons. We equate the creation of CH_n radicals to the appropriate destruction rate of CH_4 ,

$$\frac{dN_{CH_n}}{dt} = \Phi_{CH_4} - \left(\frac{dN_{CH_4}}{dt}\right)_{ions} - \left(\frac{dN_{CH_4}}{dt}\right)_{ox} \geq 0. \quad (27)$$

We equate the production of oxidizing radicals in the haze-forming regions to the appropriate photolysis rates of H_2O and CO_2 ,

$$\frac{dN_{ox}}{dt} = \Phi_{CO_2} + \Phi_{CO_2}^* + \Phi_{H_2O} \geq 0. \quad (28)$$

We assume that C_2H_n molecules form when a CH_n radical reacts with another CH_n radical, while CO forms when a CH_n radical reacts with an O or OH radical,

$$\frac{dN_{C_2H_n}}{dt} = \frac{1}{2} \frac{dN_{CH_n}}{dt} \left(\frac{dN_{CH_n}/dt}{dN_{ox}/dt + dN_{CH_n}/dt}\right)^2. \quad (29)$$

Organic hazes form when several CH_n radicals react with the growing polymer for each reaction with an O or OH,

$$\frac{dN_{\text{haze}}}{dt} = \frac{dN_{\text{CH}_x}}{dt} \left(\frac{dN_{\text{CH}_x}/dt}{dN_{\text{Ox}}/dt + dN_{\text{CH}_x}/dt} \right)^m. \quad (30)$$

For specificity, we take $m = 5$ (corresponding to six carbons). For accounting purposes, we assume that all hazes fall to the surface and accumulate without further reaction,

$$N_{\text{haze}} = \int \frac{dN_{\text{haze}}}{dt} dt. \quad (31)$$

Hazes are generally ineffective at shielding molecules from photolysis at wavelengths where an abundant gas absorbs strongly, because hazes make up a very small mass fraction of the atmosphere. Where hazes can matter is in shielding a gas of very low abundance at wavelengths that would otherwise be transparent. The cases of interest here are H_2O , which can be cold-trapped, and NH_3 .

4.1.5. CO and CO_2 Budgets

The CO_2 budget is a balance between photolytic losses and CO oxidation,

$$\begin{aligned} \frac{dN_{\text{CO}_2}}{dt} = & -\Phi_{\text{CO}_2}(1 - f_{2x}f_{35}) - \Phi_{\text{CO}_2}^* + f_{35}\Phi_{\text{H}_2\text{O}} \\ & + \Phi_{\text{CO}_2}(1 - f_{2x}f_{45}) \end{aligned} \quad (32)$$

where f_{2x} denotes the fraction of $\text{O}(^1\text{D})$ that reacts with other atmospheric species to create OH radicals,

$$f_{2x} \equiv \frac{k_{21}N_{\text{H}_2} + k_{22b}N_{\text{CH}_4} + 2k_{23}N_{\text{H}_2\text{O}}}{\sum_j k_{2j}N_j}, \quad (33)$$

f_{35} is the fraction of OH radicals that react with CO,

$$f_{35} \equiv \frac{k_{35}N_{\text{CO}}}{\sum_j k_{3j}N_j}, \quad (34)$$

and f_{45} is the fraction of ground-state O atoms that react with CO to make CO_2 ,

$$f_{45} \equiv \frac{k_{45}N_{\text{CO}}}{\sum_j k_{4j}N_j}. \quad (35)$$

The latter reaction, although spin-forbidden, is important at high pressure in a dry CO-rich atmosphere in the absence of catalysts.

The CO budget reverses the CO_2 budget and also includes the net oxidation of CH_4 as a source,

$$\frac{dN_{\text{CO}}}{dt} = -\frac{dN_{\text{CO}_2}}{dt} - \frac{dN_{\text{CH}_4}}{dt} - \frac{dN_{\text{haze}}}{dt} - \frac{dN_{\text{HCN}}}{dt}, \quad (36)$$

while treating precipitation of organic hazes and nitriles as a carbon sink.

This model of CO and CO_2 gives a better description of the sum of CO and CO_2 than it does of CO and CO_2 individually. Within the model, speciation between CO and CO_2 is sensitive to H_2O (the only oxidant). We suspect that our model overpredicts CO at the expense of CO_2 .

4.1.6. Nitrogen and HCN Budgets

In the anoxic atmospheres relevant to this study, nitrogen chemistry leads either to nitriles (e.g., HCN) or to the reconstitution of N_2 . The direct products of nitrogen photolysis are

$$\frac{dN_{\text{N}}}{dt} = \Phi_{\text{N}_2} \left(1 + \frac{k_{15}N_{\text{CO}} + k_{16}N_{\text{N}_2}}{\sum_j k_{1j}N_j} \right), \quad (37)$$

$$\frac{dN_{\text{NO}}}{dt} = \Phi_{\text{N}_2} \frac{k_{13}N_{\text{H}_2\text{O}} + k_{14}N_{\text{CO}_2}}{\sum_j k_{1j}N_j}, \quad (38)$$

$$\frac{dN_{\text{NH}}}{dt} = \Phi_{\text{N}_2} \frac{k_{11}N_{\text{H}_2} + k_{12b}N_{\text{CH}_4}}{\sum_j k_{1j}N_j}, \quad (39)$$

and

$$\frac{dN_{\text{H}_2\text{CN}}}{dt} = \Phi_{\text{N}_2} \frac{k_{12a}N_{\text{CH}_4}}{\sum_j k_{1j}N_j}. \quad (40)$$

The H_2CN radical leads to HCN. Reaction paths through NO and HNO end in reactions with N that reconstitute N_2 . These are the most important paths when CO_2 is abundant. The NH radical can be important when H_2 is very abundant, but under these circumstances, NH is more likely to be recycled to N_2 than to react with CH_n to form C–N bonds. Ground-state N reacts quickly with CH_n to make HCN, or if CH_n is not abundant, it can be recycled to N_2 through reactions with NH or NO, or following reaction with OH. For most cases of interest here, OH is strongly suppressed by reactions with abundant CO or H_2 .

Ammonia can be abundant after some impacts. As a placeholder, we assume that it is photolyzed

$$\frac{dN_{\text{NH}_3}}{dt} = -\Phi_{\text{NH}_3}. \quad (41)$$

If methane is also abundant, ammonia photolysis probably leads to amines, but if H_2 is more abundant, ammonia photolysis will mostly end with reconstitution of N_2 . The fraction of NH_3 photolyses that lead to amines or nitriles is approximated by

$$f_{99} = \frac{dN_{\text{CH}_4}/dt}{dN_{\text{CH}_4}/dt + \Phi_{\text{H}_2\text{O}} + \Phi_{\text{CO}_2}}. \quad (42)$$

Reactions of NH_n with H_2 will reconstitute NH_3 and can be ignored. Efficient formation of cyanamide (NH_2CN) may require NH_3 .

Net HCN, nitrile, and amine production is approximated by

$$\frac{dN_{\text{HCN}}}{dt} = 2\Phi_{\text{N}_2}f_{1x} \left(\frac{dN_{\text{CH}_x}/dt}{2\Phi_{\text{N}_2}f_{1x} + dN_{\text{CH}_x}/dt} \right) + f_{99}\Phi_{\text{NH}_3}. \quad (43)$$

where f_{1x} represents the fraction of excited $\text{N}(^2\text{D})$ atoms produced that are available to make HCN,

$$f_{1x} = \frac{k_{12}N_{\text{CH}_4} + k_{15}N_{\text{CO}} + k_{16}N_{\text{N}_2}}{\sum_j k_{1j}N_j}. \quad (44)$$

Equation (43) understates the possibility of NH reacting with organic species to make nitriles or amines. The corresponding net loss of N_2 by photolysis is

$$\frac{dN_{\text{N}_2}}{dt} = -\Phi_{\text{N}_2} + \frac{1}{2} \frac{dN_{\text{HCN}}}{dt} + \frac{1}{2} \Phi_{\text{NH}_3}(1 - f_{99}). \quad (45)$$

A convenient simplification is that these are reduced atmospheres with no net production of nitrogen oxides.

The chief chemical sinks of HCN are addition reactions with OH and H. The direct reaction with OH has an exothermic branch with products CO and NH₂, but the substantial rearrangements required to get these products require leaping over two energy barriers (Dean & Bozzelli 2000). The climb over the first barrier gives, as one possible set of products, atomic H and HNCO (isocyanic acid). Addition reactions with H or CH_n can lead eventually to full hydrogenation through various intermediates including cyanamide and methyamine. Like oxidation, these paths are expected to be kinetically inhibited.

The important physical sink is rainout. HCN is not very soluble in water (its Henry Law coefficient is not very high) but it is miscible. Total nitrile production is approximated by

$$N_{\text{HCN}} = \int \frac{dN_{\text{HCN}}}{dt} dt. \quad (46)$$

4.1.7. Hydrogen and Hydrogen Escape

The most important loss process for hydrogen is escape and its most important sources are CH₄ photolysis and oxidation, and water photolysis. Zahnle et al. (2019) found that, for a wide range of solar EUV fluxes and hydrogen mixing ratios, hydrogen escape from a terrestrial CO₂-H₂ atmosphere can be approximated by

$$\left(\frac{dN_{\text{H}_2}}{dt}\right)_{\text{esc}} \approx -\frac{AS_1}{\sqrt{1+B^2S_1^2}} \frac{N_{\text{H}_2}}{\sum_j N_j} \text{ cm}^{-2} \text{ s}^{-1}. \quad (47)$$

where $A = 2 \times 10^{12} \text{ cm}^{-2} \text{ s}^{-1}$ and $B^2 = 0.006$. Here, we use S_1 from Table 2 to scale EUV radiation to the levels appropriate to the young Sun. Equation (47) blends the energy-limited escape (the limit where S_1 is small) with the diffusion-limited escape (the limit where S_1 is large). Photochemical destruction of H₂ is not a concern for the hydrogen budget because in the diffusion limit, H and H₂ escape almost equally easily.

Equation (47) is readily generalized to other planets and other atmospheric compositions by recognizing that A is proportional to the density of the planet and $A \div B = b_{ia}(H_a^{-1} - H_{\text{H}_2}^{-1})$, where H_{H_2} and H_a represent the unperturbed scale heights of H₂ and the background static atmosphere at the homopause, and b_{ia} represents the binary diffusivity between H₂ and the background atmosphere. The latter is roughly the same for CO₂, CO, N₂, and CH₄ (Marrero & Mason 1972). We can ignore H_{H_2} at this level of approximation. Thus, for Earth, $B \propto m_a \div m_{\text{CO}_2}$, where the mean molecular mass of the static gases is

$$m_a = \frac{\sum_j N_j m_j - N_{\text{H}_2} m_{\text{H}_2}}{\sum_j N_j - N_{\text{H}_2}}. \quad (48)$$

Other things equal, the diffusion-limited hydrogen escape rate is about three times greater in CO₂ than in CH₄. We take the variation of B as a function of m_a into account in our models.

Sources of H₂ are photochemical or geological. The direct source is methane: each methane lost creates the equivalent of two H₂ molecules. Another source of H₂ is the water that oxidizes carbon from CH₄ to CO and CO₂. In evaluating this source, we hold H₂O constant. The presumption is that water is in equilibrium with an ocean and re-supplied to the stratosphere as needed. Some hydrogen is removed from the atmosphere

when it is incorporated in precipitating organics and nitriles. For these, we assume an H/C ratio of unity. The total rate of change of hydrogen is then

$$\begin{aligned} \frac{dN_{\text{H}_2}}{dt} = & \left(\frac{dN_{\text{H}_2}}{dt}\right)_{\text{esc}} - 2\frac{dN_{\text{CH}_4}}{dt} + 2\frac{dN_{\text{CO}_2}}{dt} + \frac{dN_{\text{CO}}}{dt} \\ & - \frac{dN_{\text{haze}}}{dt} - \frac{dN_{\text{HCN}}}{dt}. \end{aligned} \quad (49)$$

4.2. Photochemical Results

Here, we present some illustrative examples of photochemical evolution for impacts of several scales.

4.2.1. Vestas

A Vesta-scale impact is at the upper limit of what life might survive or prebiotic biomolecules might survive. Vesta itself is 525 km diameter and has about 1% of the mass of the entire late veneer. There is energy enough to evaporate two oceans of water, which leaves few refugia unless the oceans were comparably enlarged.

Figure 6 shows evolution after a Vesta-size impact into a hefty pre-impact atmosphere holding 5 bar of CO₂ and 1 bar of N₂, and 1.85 oceans (500 bar) of H₂O. If all of the Fe is used, the impact creates 3.9 bar of H₂ and converts about 9% of the 5 bar of CO₂ into CH₄ (see Table 1). Subsequent photochemical evolution assumes 1 ppm H₂O in the stratosphere, slightly drier than modern Earth's. Production rates of HCN, C₂H_n species, and haze are roughly 30× larger than those on modern Titan, or comparable to modern volcanic emissions of SO₂ or modern lightning production of NO. Cumulative precipitation of organics is about 5 cm. Hydrogen equivalent to 45 m of a global ocean escapes to space over the course of the event.

We estimate the surface temperature by assuming that the troposphere follows a moist adiabat, with the tropopause at the skin temperature,

$$\begin{aligned} T_{\text{surf}} & \approx \left(\frac{(1-A)SF_{\odot}}{8\sigma_B}\right)^{0.25} \left(\frac{P_{\text{surf}}}{P_{\text{tr}}}\right)^{(\gamma-1)/\gamma} \\ & = 180 \left(\frac{P_{\text{surf}}}{0.1 \text{ bar}}\right)^{0.13} \text{ K}. \end{aligned} \quad (50)$$

We put the tropopause at 0.1 bar, as it is in most solar system planets with atmospheres (Robinson & Catling 2014). The solar constant $F_{\odot} = 1.36 \times 10^6 \text{ erg cm}^{-2} \text{ s}^{-1}$ and the Stefan-Boltzmann constant $\sigma_B = 5.67 \times 10^{-5} \text{ erg cm}^{-2} \text{ s}^{-1} \text{ K}^{-4}$. Earth's modern surface temperature is recovered with albedo $A = 0.3$ and $\gamma = 1.15$. For early Earth, the young Sun is 72% as bright as the modern Sun ($S = 0.72$). If we take $0.3 < A < 0.5$, the ~6 bar atmosphere (1.6 bar CO₂, 0.55 bar N₂, 3.9 bar H₂, 0.17 bar CH₄) implies a surface temperature $T_{\text{surf}} \sim 320 \text{ K}$. A proper radiative-moist-convective model would be required to provide better estimates of surface temperature and tropopause conditions.

Figure 7, a more productive scenario than Figure 6, is obtained if the reducing power of FeO in pre-existing mantle and crust is exploited by lowering the quench temperature to the critical point of water and imposing the QFM buffer, as discussed above in the context of Figure 5. For a Vesta-size impact striking 2 bar of CO₂, 1 bar of N₂, and 1.85 oceans

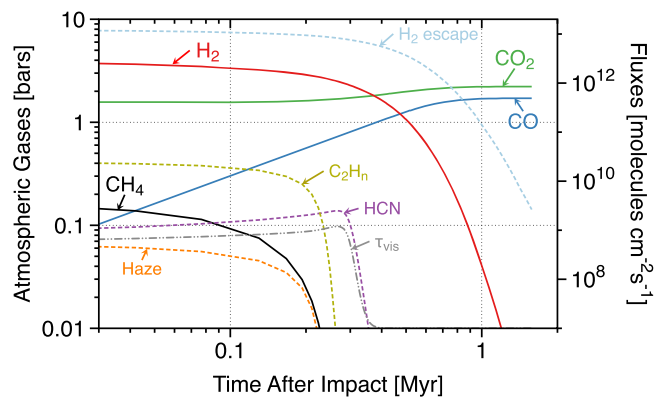


Figure 6. Photochemical dissipation of an atmosphere after the impact of a Vesta-sized body. The pre-impact atmosphere contained 5 bar of CO₂ and 1 bar of N₂ over 1.85 oceans (500 bar) of H₂O. This example assumes a dry (1 ppm H₂O) stratosphere. The optical depth of organic hazes at 564 nm τ_{vis} is shown against the left-hand axis. Production rates of HCN, C₂H_n species, and haze are plotted against the right-hand axis. The H₂ escape flux is also plotted against the right-hand axis. Note that in this case, nitrile production (“HCN”) continues well after the other hydrocarbons have dissipated; the residual optical depth—of order unity at 250 nm—is from nitrogenous hazes.

(500 bar) of H₂O, the result is 1.8 bar of H₂ and conversion of more than 90% of the CO₂ into CH₄ and more than 10% of the nitrogen into ammonia (see Table 1). The subsequent photochemical evolution in Figure 7 assumes a dry 0.1 ppm H₂O stratosphere. Such dryness might be expected in a deep greenhouse atmosphere illuminated by the faint young Sun. Predicted production rates of HCN, C₂H_n species, and haze are roughly 1000× larger than those on modern Titan for about 0.7 Myr. Cumulative precipitation of organics is about 10 m. Hydrogen equivalent to 60 m of a global ocean escapes to space over the course of the event.

4.2.2. A “Pretty Big” Impact

Figures 8 and 9 document the profound influence of stratospheric moisture on atmospheric evolution after a bigger impact, here a “pretty big” 2.5×10^{24} g EH-type body striking a 5 bar CO₂, 1 bar N₂ atmosphere over 1.85 oceans (500 bar) of liquid H₂O. This approximates the largest event in a minimum late veneer extrapolated from the lunar cratering record, as discussed in Section 2 above. The surface temperature before the impact may have been in the range $310 < T < 340$ K (estimated using Equation (50)). There is enough energy released by the impact to vaporize 20 oceans of water or melt the crust to a depth of tens of kilometers. It seems unlikely that life on Earth could survive the immediate effects of an impact of this scale, but surface conditions 10,000 years later are plausibly temperate enough. This is an interesting scale for setting the table for life of the future (Benner et al. 2019a).

If all of the new iron reacts with water and CO₂, this impact generates 8.4 bar of H₂ and converts nearly all 5 bar of CO₂ into 0.4 bar of CH₄. The mean molecular weight of the air is 3 and the scale height is 100 km. These are hydrogen atmospheres resembling Neptune’s more than modern Earth’s. Viewed in transit, such an atmosphere would add about 10% to Earth’s apparent diameter, or put another way, it would lead a distant observer to conclude that Earth had a density of just 4 g cm⁻³.

The photochemical evolution in Figure 8 assumes 1 ppm H₂O in the stratosphere. The outcome is somewhat similar to that following the Vesta impact, differing mostly in the lack of CO₂. Most of the methane is eventually oxidized. A small

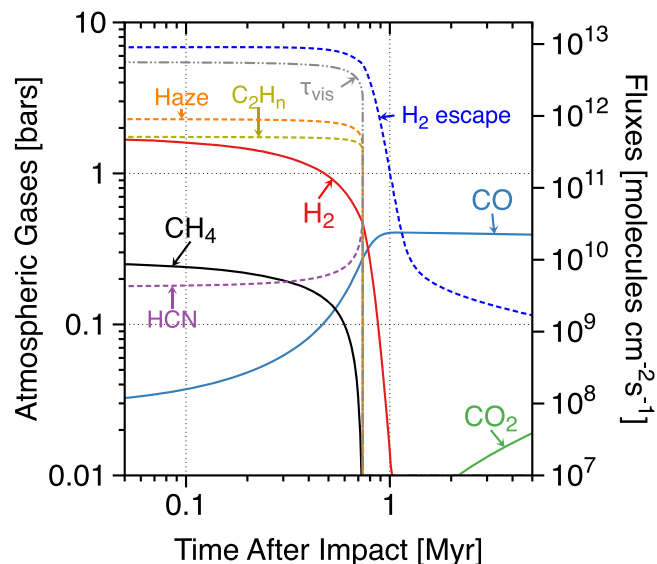


Figure 7. Photochemical evolution after a Vesta-size impact assuming that the atmosphere and ocean equilibrate with the QFM buffer at 650 K (see Figure 5). The pre-impact atmosphere contained 2 bar of CO₂; otherwise, conditions are the same as for Figure 6. The case is listed in Table 1.

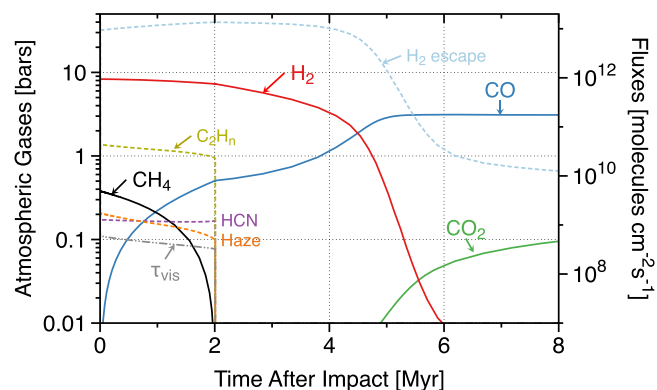


Figure 8. Photochemical dissipation of an atmosphere perturbed by a pretty big 2.5×10^{24} g impact. The pre-impact atmosphere contained 5 bar of CO₂ and 1 bar of N₂ over 1.85 oceans (500 bar) of H₂O. Partial pressures are shown against the left-hand axis. This example assumes 1 ppm H₂O in the stratosphere, like Earth today. Production rates of hazes, C₂H_n species, and HCN are indicated against the right-hand axis. The H₂ escape flux is also plotted against the right-hand axis. Hydrogen from 50 bar (0.2 oceans, 500 m) of H₂O escapes over the course of the event.

fraction of the CH₄ is built up into organics, nitriles, and hazes. Production of HCN, hazes, and C₂H_n organics is roughly 10 times faster than on modern Titan. Cumulative precipitation of hazes and nitriles is of the order of half a meter, with perhaps another half-meter of partially oxidized organic matter (e.g., organic acids and aldehydes stemming from partial oxidation of hydrocarbons). Hydrogen from 50 bar (0.2 oceans, 500 m) of H₂O escapes over 4 Myr. Oxidation in the dry stratosphere is too slow to convert CO to CO₂ on the timescale of this event.

Figure 9 is the same impact as Figure 8, but evolving with a stratosphere that is 10 times drier (0.1 ppm H₂O). The drier stratosphere might be appropriate given the strong greenhouse effect of the deep troposphere and the faint Sun. The outcomes are quite different. The low rates of stratospheric H₂O photolysis frustrate oxidation of small organics and, thus, allow the buildup of thick photochemical hazes ($\tau_{\text{vis}} \sim 5$ at 560 nm according to the fractal model). In this example, fully 60% of the

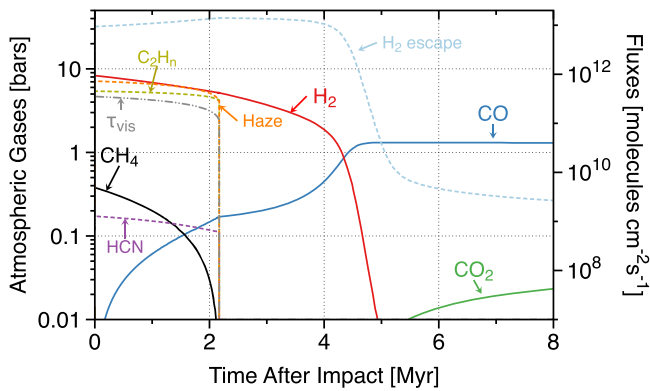


Figure 9. Same as Figure 8 but drier (0.1 ppm stratospheric H₂O). Organic hazes form with optical depths of order 3–5 at 564 nm (τ_{vis}). Haze optical depth is plotted against the left-hand axis. In this example, production rates of HCN and C₂H_n species, indicated against the right-hand axis, are very large, about 500× what they are on modern Titan, or 2% of modern biotic productivity. Cumulative organic precipitation is of the order of 100 moles cm⁻².

impact-generated CH₄ is converted into organic precipitates (hazes), which correspond in cumulate to a global blanket 10–20 m thick. On the other hand, production of organic nitrogen is no greater because in both cases, it is limited by the rate of N₂ photolysis. Conditions gradually grow less, reducing until the methane is fully titrated and an abrupt bleaching event clears the skies. In the end, about 40% of the CH₄ is oxidized to CO, and the hydrogen from 0.15 oceans of H₂O escape to space.

4.2.3. The “Maximum HSE” Impact

Other things equal, there is a small but significant statistical chance, of the order of 10%, that the last of the world-sterilizing events was also the biggest of them. Surface environments will not be habitable until well after the impact, but much can be done to prepare the planet for a more hopeful future. This approximates the impact discussed by Benner et al. (2019a).

We document two versions of a maximum HSE event, one with a very dry stratosphere and one somewhat moister. The simulations presume the impact on Earth of a highly reduced Pluto-sized dwarf planet, at a time after the Moon-forming impact when there were still 100 bar of CO₂ at the surface. Other initial conditions are 1 bar of N₂ and 1.85 oceans of water (500 bar). The biggest impact differs from smaller impacts in two key respects: there is more iron than CO₂ and H₂O at the surface, and the ejecta blanket is much deeper than the oceans. The former means that the mineral buffer should be important, while the latter hints that much of the metallic iron might at first be buried.

For specificity, we presume that the atmosphere and ocean equilibrate with the IW mineral buffer and that the remaining metallic iron is oxidized later on geological timescales. With these particular assumptions, the impact converts all of the CO₂ and 15% of the water to CH₄. About 60% of the water (one ocean) remains as H₂O. Expressed in moles, the atmosphere after the impact contains 6000 moles H₂ per cm² (40% of the hydrogen in Earth’s current oceans) and 2300 moles CH₄ per cm². Expressed as pressure, after the impact, the dry atmosphere would at first hold 35 bar of H₂ and 14 bar of CH₄, with a mean molecular weight of 6. Because the surface temperature would be high, a great deal of water would remain in the vapor phase, and the actual mean molecular weight and partial pressures of H₂ and CH₄ would be correspondingly higher.

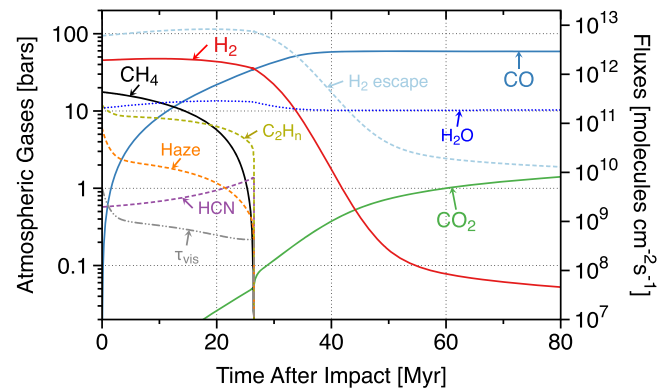


Figure 10. Photochemical evolution of a maximum HSE impact-generated atmosphere assuming 1 ppm H₂O in the stratosphere. Initial conditions (100 bar CO₂, 1.85 oceans of water) may be appropriate to the largest of Earth’s post-Moon impacts. Partial pressures are shown against the left-hand axis. Water vapor is mostly confined to the troposphere and presumes a surface temperature governed by total atmospheric pressure according to Equation (50). Organic C₂H_n, HCN, and haze production (dashed curves) are mapped to the right-hand axis. The rate of hydrogen escape is also mapped to the right-hand axis. Haze optical depth at 560 nm (τ_{vis}) is plotted against the left-hand axis.

Figure 10 documents photochemical evolution with an Earth-like (1 ppm H₂O) stratosphere. As with the pretty big impacts, this stratosphere is moist enough that oxidation following water photolysis is more important than polymerization of CH₄. The photochemical source of organic matter (C₂H_n, HCN, haze) is nonetheless large, of the order of 100× that of modern Titan. This case generates a cumulative global blanket of 25 m of haze organics, plus another 5 m of partially oxidized organics and 5 m of nitrogen-rich organics. Much of the nitrogenous material would be amines stemming from impact-generated NH₃. The hydrogen from 2.3 km of water escapes (leaving one ocean of water behind). Cases with still wetter stratospheres closely resemble this one.

Figure 11 documents photochemical evolution with the drier (0.1 ppm H₂O) stratosphere. The dry stratosphere leads to highly reduced conditions and rapid photochemical organic haze production at 10³× the rate on modern Titan. Haze optical depths in the UV exceed 100; visible optical depths are in the range of 4–8. More than 70% of the methane is polymerized into organic matter equivalent to a cumulative deposit of the order of 300–500 m deep. In addition, about 10 m of nitrogenous material reaches the surface, much of which stems from impact-generated NH₃ that is photolyzed in the presence of abundant hydrocarbons, rather than from photochemical HCN. The rest of the methane is oxidized to CO. The hydrogen from 1.7 km of water escapes. Cases with even drier stratospheres closely resemble this one.

Despite the thick organic hazes, the climates of the post-impact atmospheres may have been dominated by the greenhouse effect from tens of bars of H₂ and CH₄ (Wordsworth & Pierrehumbert 2013), and the surface temperature may have been 350–450 K, or higher.

4.2.4. Sub-Vestas

Finally, we consider two impacts that are small enough that life or its precursors ought to survive. These have the potential to build on what may already have been accomplished. We look at two cases, the first using the same approach as we used for ocean-vaporizing impacts, and, as this turns out to be rather

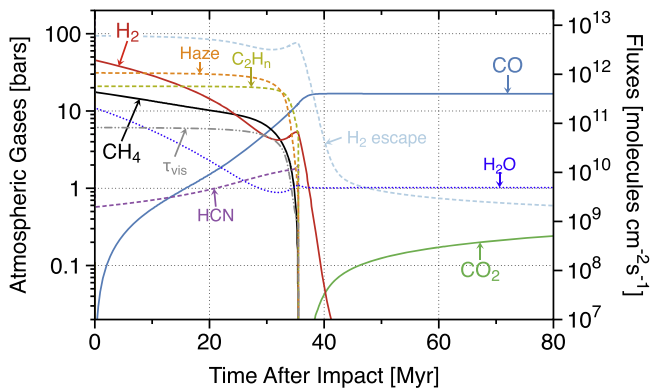


Figure 11. Same as Figure 10 but with a drier (0.1 ppm H₂O) stratosphere. Water vapor is mostly confined to the troposphere and presumes a surface temperature governed by total atmospheric pressure according to Equation (50). In this case, the evolution is characterized by a very reduced stratosphere and a great deal of Urey–Miller-like abiotic organic production that consumes most of the CH₄. Organic (C₂H_n, HCN, and haze) production rates (dashed curves) are mapped to the right-hand axis. Haze optical depth at 560 nm (τ_{vis}) is plotted against the left-hand axis.

disappointing, we consider a second case for which the assumptions are more liberal and the outcome more bountiful.

The first example, Figure 12, uses only the free Fe of the impact to reduce water and CO₂. This case assumes 5 bar CO₂ and 1 bar of N₂ in the atmosphere and 1.85 oceans of water on the surface before the impact. The impact evaporates about half the ocean, leaving deep waters less disturbed and some subsurface environments continuously habitable.

The atmosphere immediately after the impact holds 6.2 bar, mostly of H₂ and CO₂. This evolves after hydrogen escape into a 5.4 bar CO₂–N₂–CO atmosphere, with about 1 bar of CO left at the end of the simulation. For a short time, the atmosphere provides a modest source of nitriles (comparable to modern Titan), but the cumulative production of organic material over the course of the event is equivalent to just 1 mm of precipitate. Unlike many of the cases we consider, the results are independent of stratospheric H₂O, because CO₂ is the oxidant. The H₂ from 15 m of water escapes.

The alternative sub-Vesta case (Figure 13) begins with the scenario presented in Figure 5 above, in which the atmosphere and ocean equilibrate with the QFM buffer at the critical temperature of 650 K. As in Figure 5, we assume that before the impact, the atmosphere held 2 bar of CO₂ and one of N₂. The low equilibration temperature favors methane and ammonia, which are both rather abundant in a 2.3 bar atmosphere volumetrically dominated by 1.5 bar of H₂ (see Table 1); although, most of the mass is in CH₄, CO₂, and N₂. For the photochemical evolution, we assume a dry stratosphere (0.1 ppm H₂O).

The story told in Figure 13 is eventful. At first, the atmosphere still holds enough CO₂ to be weakly oxidizing and organic production is modest, but after the CO₂ is gone, stratospheric conditions become much more reduced, and organic production becomes considerable and stays so for about 0.5 Myr. This second phase ends abruptly when the methane disappears. Cumulative production of organics is in the range of 2.5–5 m of hydrocarbons and nitriles. The H₂ from 40 m of water escapes. The asymptotic state features about a bar of N₂ and CO each, the latter slowly oxidizing to CO₂ on geologic timescales.

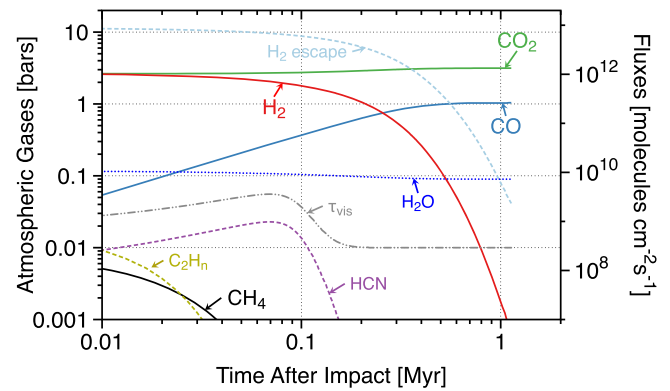


Figure 12. A non-ocean-vaporizing impact. This case assumes 5 bar CO₂ and 1 bar of N₂ before the impact. Quenching is determined by gas-phase reactions. Partial pressures (solid curves) are plotted against the left-hand axis, while fluxes (dashed curves) are plotted against the right-hand axis. Note the prolonged production of HCN in clear skies.

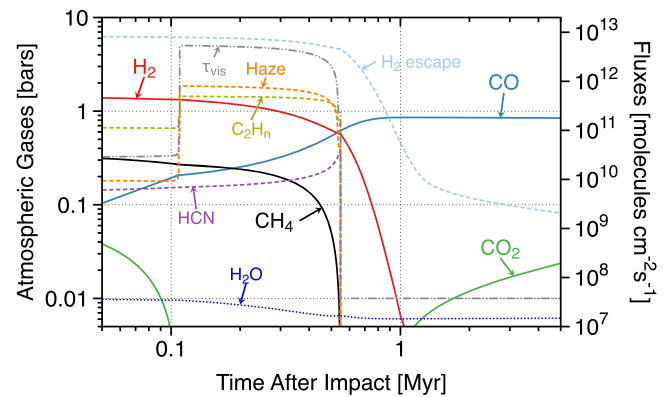


Figure 13. A non-ocean-vaporizing impact that assumes that the atmosphere and ocean equilibrate with the relatively oxidizing QFM buffer at 650 K (i.e., at water's critical temperature). Quenching is not determined by gas-phase reactions. This case assumes 2 bar of CO₂ and 1 bar of N₂ before the impact. Partial pressures are shown.

5. Discussion

Benner et al. (2019a) have suggested that the greatest of the late veneer impacts (corresponding to those we simulate in Section 4.2.3) created a transiently reducing surface environment on Earth ca. 4.35 Ga and that this environment lasted for about 15 million years. They also suggest that the origin of the RNA world dates to this interval. They emphasized the difficulty in generating the simple N-rich organic molecules like cyanoacetylene and cyanamide needed to make purines and pyrimidines by paths other than highly reducing atmospheric chemistry. Although the dates and timing of events are less certain than Benner et al. (2019a) seem to suggest, in broad brush, we find ourselves in general agreement. The quantity of reducing power is determined from the excess HSEs in the mantle. The timescale is set by the EUV radiation emitted by the young Sun. With due allowance for the uncertainty in both, a timescale in the general range of 10–100 Myr is obtained by simply dividing one quantity by the other, and it cannot be hugely wrong. As to when these events took place, opinions can differ, depending on how much weight one places on the ability of zircons to record the evolving conditions at the Earth's surface (Carlson et al. 2014).

A possible problem posed by the biggest impact is that, although it brings the most reducing power, it is also the most likely to leave the surface too hot to promote prebiotic

evolution, and for a long time. Even ignoring CO₂ and CH₄, the greenhouse effect provided by tens of bars of H₂ could raise the surface temperature to 400 K or more. Adding CO₂ or CH₄ or other greenhouse gases would make the surface still hotter. Impacts that are 10- to 100-fold smaller may therefore seem preferable, as these are more likely to leave the surface in a temperate state, albeit the reducing conditions do not last as long as for the bigger events. In a more recent study, Benner et al. (2019b) concede the potential advantages of less enormous impacts, while making a new point: the transience of highly reduced impact-generated atmospheres lets the prebiotic system exploit other chemical pathways pertinent to the RNA world that work better in weakly reduced (QFM mantle-derived) atmospheres. These make use of volcanic SO₂ (S in a deeply reduced atmosphere would be in H₂S), borates, and even the highly oxidized Mo⁺⁶.

An important opportunity that we have not quantitatively addressed is the delayed oxidation of impactor metallic iron that escaped immediate oxidation by the ocean or atmosphere. This iron would instead have been oxidized by recycled surface volatiles over the course of geologic time, which may have been millions or many tens of millions of years. If the chief oxidant were water, the chief volcanic gas would have been H₂. But if the chief oxidant were CO₂ (probably in the form of subducted carbonate), volcanic gases could have included significant amounts of the much more useful CH₄. Methane abundances are sensitive to pressure, but to give a specific example, CH₄ becomes the most abundant C-containing gas at the QFI buffer at 1400 K under 300 bar pressure, and it is still 10% at 1600 K. In the latter regime—one in which CO₂ must have been abundant in the atmosphere (else no carbonate) and CH₄ was abundant in undersea volcanic gases—the chief photochemical products would have been HCN and small organic acids, aldehydes, and carbonyls. This regime could have lasted for a long time, possibly tens of millions years or more.

5.1. Ammonia

Large impacts can generate considerable amounts of ammonia from hot H₂ and N₂. Ammonia's fate involves many processes that are more complex than what we have been considering in this study. Nonetheless, the inherent interest of ammonia as a constituent of the prebiotic environment is great enough that we will risk some speculations.

Ammonia is highly susceptible to UV photolysis at 185 < λ < 215 nm, where its cross section is of the order of 3 × 10⁻¹⁸ cm², at wavelengths where the solar photon flux is much higher than at the shorter wavelengths where H₂O and CO₂ absorb. The products are NH and NH₂ radicals (Huebner et al. 1992) that swiftly react with each other, with oxygen, or with hydrogen in a series of reactions that efficiently recombine N₂ (Kuhn & Atreya 1979). Without the protection of high-altitude UV absorbers, a bar of NH₃ would revert to N₂ in less than 10⁴ yr on early Earth.

However, if the atmosphere were also CH₄-dominated, as it likely would be were NH₃ abundant, the resulting hydrocarbon hazes might provide UV protection (Sagan & Chyba 1997). Perhaps more important is that a significant fraction of the NH and NH₂ radicals that photolysis creates will have good odds of reacting with hydrocarbons to make amines and nitriles. Under these conditions, the coupled hydrocarbon-ammonia photochemistry would lead to amines and nitriles (Miller 1953).

The other factor to consider with ammonia is that it is very soluble in cool water and, hence, likely to rain out and partition into the ocean. The Henry's Law coefficient for NH₃ in water is $K_H = 4.6 \times 10^{-5} e^{-4200/T}$ moles l⁻¹ atm⁻¹. Much of the dissolved NH₃ hydrolyzes to ammonium, NH₄⁺. Ammonium abundance is related to NH₃(aq) and pH by

$$[\text{NH}_4^+][\text{OH}^-] = K_b[\text{NH}_3] \quad (51)$$

in which the base constant K_b is a weak function of temperature (Read 1982),

$$\log(K_b) \approx -4.75 - 2.5 \times 10^{-5}(T - 298). \quad (52)$$

Expressing [OH⁻] in terms of pH and the auto-ionization constant K_w of water (which can be crudely approximated as a function of T by $\log(K_w) = -14 + 0.03(T - 298) - 7.5 \times 10^{-5}(T - 298)^2$), the ammonium/ammonia ratio is

$$\log\{[\text{NH}_4^+]/[\text{NH}_3]\} = \log(K_b) - \log(K_w) - \log(\text{pH}). \quad (53)$$

If all of the nitrogen currently in Earth's atmosphere were converted to NH₃, the equilibrium NH₃ gas pressure above an ocean with pH of 7.8 and temperature 298 K would be just 100 mbar (yet enough to generate a considerable greenhouse effect). The other 1.56 bar of N would be dissolved in the oceans, 97% as NH₄⁺.

Hotter oceans are interesting. At 373 K, other things equal, the NH₄⁺/NH₃ ratio would drop to ~2. The equilibrium NH₃ gas pressure over the ocean would be 0.02 bar. The other 1.54 bar of NH₃ would be in the oceans, divided between NH₄⁺ and NH₃. At 500 K, the pH would be another unit lower, and NH₄⁺ less abundant than NH₃. The equilibrium NH₃ gas pressure in the atmosphere rises to 0.7–1.0 bar, with the rest of the N divided between NH₃ and NH₄⁺ dissolved in the ocean. In this case, the ammonia would probably be photochemically destroyed very quickly, although many of the products would be prebiotically interesting if CH₄ were also abundant.

This exercise suggests that NH₃ would last the longest as ammonium ions in cold seas under an organic haze, conditions rather similar to those sometimes imagined for early Titan. We speculate that ammonia's powerful greenhouse effect can lead to a strong positive feedback between ocean temperature and exsolution that would in turn speed ammonia's photochemical destruction. It is not obvious that keeping ammonia around for a long time is a better option for prebiotic purposes than a rapid dump of a wide variety of nitrogenous products into warm oceans. Here, we simply present these cases as end-members.

5.2. The Hadean Impact Cascade

Figure 14 presents a notional history of water, methane, and HSEs on early Earth in response to late great impacts. The last stage of this impact history is evident on the face of the Moon and is often called the "late heavy bombardment," often referred to as the "LHB." Water on Earth probably accreted before the Moon-forming impact, and the quantity of water on Earth was likely to have decreased during the late accretion of what the isotopic evidence shows were mostly water-poor bodies. Transient methane-rich atmospheres are generated by ocean-vaporizing impacts. Here, we presume that the mantle's excess HSEs were delivered mostly by a single impact, with light shading indicating an allowance for the HSEs dating to the Moon-forming impact itself. Major impacts are shown decreasing in magnitude as time passed, but the true order

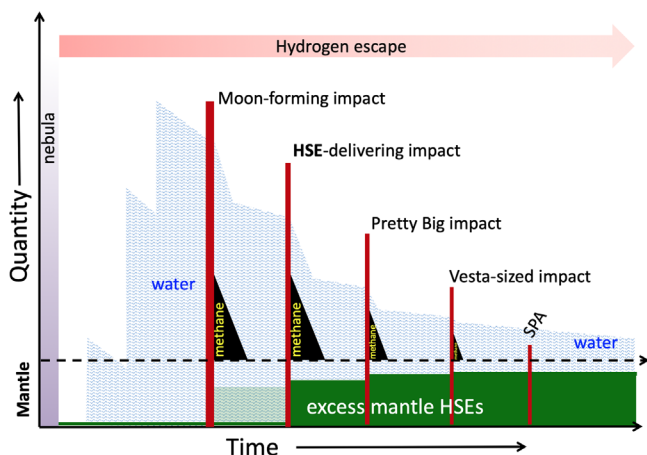


Figure 14. A schematic history of water, methane, and highly siderophile elements on Earth in response to late great impacts. “SPA” refers to an impact on the scale of the one that excavated the lunar S. Pole–Aitken basin—too small to evaporate the oceans—which is implied here by submerging SPA’s pole under the waves. Major impacts are shown decreasing in magnitude as time passed, but the true order leaves much to chance; it is possible that the largest of the ocean-vaporizers was also the last.

leaves much to chance; it is possible that the largest of the ocean-vaporizers was also the last. Each great impact left Earth in a state resembling somewhat the state of early Earth as sketched by Urey (1952) for periods that may have been less than a million years or as long as 100 million years, the duration depending on the size of the impact and on the flux of ultraviolet radiation from the young Sun.

6. Conclusions

Great impacts of Earth’s late accretion—especially those that evaporated the oceans—differ from lesser impacts in several important ways. First, they delivered significant reducing power in the form of metallic iron to Earth’s surface environments. We infer this because the characteristic isotopic fingerprints of the mantle’s HSEs establishes the late veneer as kin to the enstatite chondrites, aubrites, and type IAB iron meteorites, all of which are profoundly reduced and bear ample metallic iron. The iron was oxidized in the crust or mantle, which we know because the HSEs are unfractionated, and hence, there was no significant loss of metal to the core. Water and CO_2 were the plausible oxidants; hence, hydrogen, carbon monoxide, and methane were the plausible products. Second, the high H_2O and H_2 vapor pressures in a reduced steam atmosphere favor CH_4 and NH_3 over CO or N_2 , a preference that goes as the square of the pressure. Third, cooling after impact was slow because the thermal inertia of a hot steam atmosphere containing hundreds of bars of gas is large. It takes more than 1000 years to cool 270 bar (an ocean) of steam at the runaway greenhouse cooling rate. The result is that quench temperatures for gas-phase reactions in the $\text{CH}_4\text{--CO--CO}_2\text{--H}_2\text{O--H}_2$ system drop to ~ 800 K or less, and quench temperatures for the $\text{NH}_3\text{--N}_2\text{--H}_2\text{O--H}_2$ system drop to ~ 1100 K. Hence, both methane and ammonia form directly by gas-phase reactions.

How much methane actually forms depends on how much carbon was available to the atmosphere before the impact, on how much reducing power was delivered by the impact, how much of the delivered iron reacts with the atmosphere and ocean as opposed to being deeply buried under the ejecta, and on whether catalysts were active to reduce the quench temperature

still further. In addition to atmospheric CO_2 and CO , available carbon inventories would include any CO_2 dissolved in the oceans, and any CO_2 in carbonate rocks that were not buried too deeply to be liberated by shock heating. Methane production could have been enormous. If, for example, we presume that a maximum-late-veener scale impact took place on an Earth with a 100 bar of CO_2 atmosphere (perhaps left over from the Moon-forming impact; Zahnle et al. 2007) and 5 km of water at the surface, there is enough time and reducing power to convert all of the carbon to methane, diluted in several tens of bars of H_2 . The resulting atmosphere is rather Neptune-like, with a scale height in the range of 50–100 km.

Another interesting aspect of the biggest impacts is that much of the delivered iron may have been too deeply buried in the ejecta blanket to be oxidized in the first few thousands of years after the impact. Under these circumstances, the iron must have been oxidized on a longer timescale set by broadly geological processes that govern the interchange of surface volatiles with crustal and mantle materials. Although we have not presented models of such a scenario here, we can expect that gases emitted from a mantle with extant metallic iron would be strongly reduced over an extended period of time. How important this impact coda might be to the origin of life depends on whether these gases included methane.

Earth’s hydrogen-methane atmospheres would have been physically stable—they did not blow off—but they were subject to photochemical dissipation, as both hydrogen escape and methane photolysis are effectively irreversible. The rate the atmosphere evolves is set by the flux of solar far and extreme ultraviolet radiations. Here we use a zero-D photochemical model to simulate atmospheric evolution: we count the photons and apportion their effects. We find that the biggest late veneer impacts can generate (cumulatively) as much as 500 m of organic over tens of millions of years, while smaller impacts do commensurately less in commensurately less time.

The details of atmospheric evolution of the transient reduced atmosphere are mostly determined by quantities (i.e., bigger impacts have bigger impacts), but there is one ill-constrained modeling parameter—the stratospheric water vapor mixing ratio—to which the outcomes are sensitive. Moister stratospheres are relatively oxidizing, while drier stratospheres are profoundly reducing and resemble conditions on modern Titan but sped up by a factor of 1000. We see a sharp transition in photochemical products determined by the competition between oxidation and reduction. In our models, the transition appears to take place at stratosphere H_2O mixing ratios in the range of 0.1–1 ppm, moisture levels that are not very different from Earth today. A more sophisticated model might predict a smoother transition, or a different critical water abundance for a sharp transition.

Lesser impacts are of course less impactful. Tens of smaller, non-ocean-vaporizing impacts will generate significant amounts of H_2 and CO but very little CH_4 or NH_3 unless catalysts were available to reduce the quench temperature. Hydrogen and CO are useful ingredients for a bootstrapping origin-of-life scenario in which the biochemical evolution began by catalyzing the kinds of chemical reactions that build hydrocarbons from CO and H_2 . But if the primary requirements for life are methane, ammonia, HCN , and their photochemical derivatives, only the biggest impacts or as of yet unknown chemistry will do.

From the points of view of the origin of life and biblical metaphors, the great impacts may be double-edged swords. In

their aftermath, they leave Earth primed and ready to start life under a classic Urey–Miller H₂-rich, CH₄-rich, possibly even NH₃-rich atmosphere that origin-of-life theorists have long favored. Unfortunately, at least with the biggest of them, the first act is an attempt to wipe out everything that had been accomplished before. What this suggests is that impact-generated transient atmospheres may give a planet only one highly favorable roll of the dice. Smaller, less dangerous impacts can inject significant amounts of new H₂ or CO into the system that might be capable of building on previous progress, but these smaller impacts require unidentified catalysts or unidentified chemistry to generate large amounts of CH₄ or NH₃. And even if all such conditions were met, there could not have many such impacts, probably no more than a dozen.

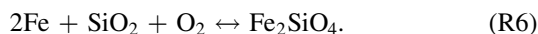
The two Fortran source codes and the BASH shells used to call the fortran codes are publicly available in a Zenodo repository at [doi:10.5281/zenodo.3698264](https://doi.org/10.5281/zenodo.3698264). These codes are built around planet characteristics specific to the early Earth. The FORTRAN codes have been compiled and tested using gfortran.

This work was in part supported by the NASA Exobiology Program, grant 80NSSC18K1082. D.C.C. was supported by the Simons Foundation. We thank Y. Abe, S. Benner, R. Carlson, S. Desch, B. Fegley Jr., V.S. Meadows, A. O’Keefe, L. Schaefer, N. H. Sleep, and J. H. Waite.

Note added in proof. Two recent papers have undermined the Ru isotopic arguments against a carbonaceous chondrite-rich late veneer. Varas-Reus et al. (2019) show that mantle Se isotopes are carbonaceous chondritic and not enstatite chondritic; this is the first convincing evidence of a substantial outer solar system contribution to the late veneer. Fischer-Gödde et al. (2020) report that Earth’s Ru isotopes are unique in the solar system, characterized by an even higher degree of s-process enrichment than the ECs or the type IAB irons. The new Ru isotopes no longer exclude a carbonaceous chondritic contribution to the late veneer. A heterogenous late veneer does not invalidate the arguments presented here, which focus on a small number of favorable events. Also, it should be understood that carbonaceous chondritic impacts are much less favorable to the in situ origin of life on Earth than more reducing impacts that interact with an ocean and generate organic matter here on Earth (Hashimoto et al. 2007).

Appendix A

We give three representative mineral buffers here. The QFI buffer is the most reduced buffer we consider,

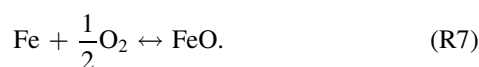


The oxygen fugacity of the QFI buffer is approximated by

$$f_{\text{O}_2} = 1.962 \times 10^{-6} T^{3.443} \exp(-54573/T - 2.073 \times 10^5/T^{1.5}). \quad (\text{A1})$$

Curve fits are based on literature fits for temperatures between $900 < T < 1420$ K. The QFI buffer is representative of many chondritic meteorites (Schaefer & Fegley 2017).

The iron-wüstite buffer (IW) is based on a simple reaction

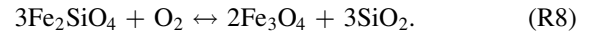


The oxygen fugacity of the IW buffer is approximated by

$$f_{\text{O}_2} = 3.1924 \times 10^{-6} T^{2.4952} \exp(-39461/T - 3.221 \times 10^5/T^{1.5}) \quad (\text{A2})$$

The direct reaction of water with iron to make FeO and H₂ seems kinetically straightforward, and hence, the IW buffer seems appropriate for the interaction of hot iron and water.

The fayalite-magnetite-quartz buffer (abbreviated FMQ or QFM) is representative of modern volcanic degassing and is regarded as typical of the modern Earth’s mantle. It is the most oxidized mineral buffer that we consider. The generic QFM reaction is



The oxygen fugacity of the QFM buffer can be approximated by

$$f_{\text{O}_2} = 3.015 \times 10^{-4} T^{3.449} \exp(-53649/T). \quad (\text{A3})$$

Oxygen fugacity f_{O_2} has units of atmospheres—we treat f_{O_2} as effectively the same as the O₂ partial pressure, p_{O_2} .

Appendix B

Table B tabulates the chemical reactions discussed in the main text.

Table B
Chemical Reactions and Rates

Reaction	Rate at 298 K cm ³ s ⁻¹
R11 N(² D) + H ₂ → NH + H	$k_{11} = 2.2 \times 10^{-12}$
R12 N(² D) + CH ₄ → products	$k_{12} = 4 \times 10^{-12}$
→ H ₂ CNH + H	$k_{12a} = 0.75 \times k_{12}$
→ NH + CH ₃	$k_{12b} = 0.25 \times k_{12}$
R13 N(² D) + H ₂ O → products ^a	$k_{13} = 5 \times 10^{-11}$
R14 N(² D) + CO ₂ → NO + CO	$k_{14} = 3.6 \times 10^{-13}$
R15 N(² D) + CO → N + CO	$k_{15} = 1.9 \times 10^{-12}$
R16 N(² D) + N ₂ → N + N ₂	$k_{16} = 1.7 \times 10^{-14}$
R21 O(¹ D) + H ₂ → OH + H	$k_{21} = 1.1 \times 10^{-10}$
R22 O(¹ D) + CH ₄ → products	$k_{22} = 1.5 \times 10^{-10}$
→ H ₂ COH + H	$k_{22a} = 0.1 \times k_{22}$
→ OH + CH ₃	$k_{22b} = 0.9 \times k_{22}$
R23 O(¹ D) + H ₂ O → OH + OH	$k_{23} = 2.2 \times 10^{-10}$
R24 O(¹ D) + CO ₂ → O + CO ₂	$k_{24} = 7.4 \times 10^{-11}$
R25 O(¹ D) + CO → O + CO	$k_{25} = 7 \times 10^{-11}$
R26 O(¹ D) + N ₂ → O + N ₂	$k_{26} = 1.8 \times 10^{-11}$
R31 OH + H ₂ → H + H ₂ O	$k_{31} = 6 \times 10^{-15}$
R32 OH + CH ₄ → CH ₃ + H ₂ O	$k_{32} = 6 \times 10^{-15}$
R35 OH + CO → CO ₂ + H	$k_{35} = 1.2 \times 10^{-13}$
R37 OH + CH ₂ → H ₂ CO + H	$k_{37} = 1.2 \times 10^{-10}$
R38 OH + CH ₃ → products	$k_{38} = 6 \times 10^{-11}$
R41 O + H ₂ → H + OH	$k_{41} = 1 \times 10^{-17}$
R42 O + CH ₄ → CH ₃ + OH	$k_{42} = 7 \times 10^{-18}$
R45 O + CO → CO ₂	$k_{45}^b = 4.0 \times 10^{-17}$
R47 O + CH ₂ → HCO + H	$k_{47} = 1.2 \times 10^{-10}$
R48 O + CH ₃ → H ₂ CO + H	$k_{48} = 1.2 \times 10^{-10}$
R57 N + CH ₂ → HCN + H	$k_{57} = 1.2 \times 10^{-10}$
R58 N + CH ₃ → H ₂ CN + H	$k_{58} = 1.1 \times 10^{-10}$
R78 CH ₂ + CH ₃ → C ₂ H ₄ + H	$k_{78} = 7 \times 10^{-11}$

Notes.

^a Products are plausibly HNO and H.

^b High-pressure limit.

Appendix C

References

Photoionizing photons (EUV₁ and S₁ in Table 2) are important for hydrogen escape but less important than photolysis for chemistry. To the first approximation, CO and N₂ usually survive photoionization intact by charge exchange. Photoionization of CO₂ usually creates CO₂⁺ ions, which can dissociate to CO after reaction with atomic H or O and can charge exchange with CH₄ to make CH₄⁺, leaving CO₂ intact while ultimately disintegrating CH₄. As we are not tracking H or O, we arbitrarily assume that 20% of CO₂ photoionizations generate CO

$$\left(\frac{dN_{\text{CO}_2}}{dt}\right)_{\text{ions}} = -0.2\Phi_{\text{CO}_2}^* \quad (\text{C1})$$

Photoionization of water usually yields H₂O⁺, which reacts with H₂ to make H₃O⁺ and H; with CH₄ to make H₃O⁺ and CH₃; and with CO to make HCO⁺ and OH. Both H₃O⁺ and HCO⁺ dissociatively recombine. The H₂O⁺ + CH₄ channel counts as a loss for CH₄, while the HCO⁺ channel counts as a source of OH. For cases of most interest to us here, H₂O will be condensed at the surface and will not be a major constituent at the top of the atmosphere, the H₂O photoionization terms will be small.

The chief chemical consequence of photoionization is that CH₄ is broken down into reactive CH_n radicals. Direct photoionization mostly yields CH₄⁺ or CH₃⁺, which, in subsequent reactions, are almost guaranteed to lead to the loss of CH₄. The other molecular ions also react with CH₄, sparking chains of reactions that lead to CH_n radicals. Exempli gratia., N₂⁺ can exchange with CO to make CO⁺, CO⁺ can exchange with CO₂ to make CO₂⁺, CO₂⁺ can react with CH₄ to free CH_n radicals. The net

$$\begin{aligned} \left(\frac{dN_{\text{CH}_4}}{dt}\right)_{\text{ions}} = & -\Phi_{\text{CH}_4}^* - \Phi_{\text{H}_2}^* \frac{N_{\text{CH}_4}}{X_1} \\ & - \Phi_{\text{CO}_2}^* \frac{N_{\text{CH}_4}}{X_3} - \Phi_{\text{CO}}^* \left(\frac{N_{\text{CH}_4}}{X_2} + \frac{N_{\text{CO}_2} N_{\text{CH}_4}}{X_2 X_3} \right) \\ & - \Phi_{\text{N}_2}^* \left(\frac{N_{\text{CH}_4}}{X_1} + \frac{N_{\text{CO}} N_{\text{CH}_4}}{X_1 X_2} + \frac{N_{\text{CO}} N_{\text{CO}_2} N_{\text{CH}_4}}{X_1 X_2 X_3} \right) \\ & + \frac{N_{\text{H}_2\text{O}} N_{\text{CH}_4}}{X_1 X_4} - \Phi_{\text{H}_2\text{O}}^* \frac{N_{\text{CH}_4}}{X_4} \end{aligned} \quad (\text{C2})$$

where the X_k factors crudely account for the branching patterns in the ion cascades:

$$X_1 = N_{\text{H}_2} + N_{\text{CH}_4} + N_{\text{H}_2\text{O}} + N_{\text{CO}} + N_{\text{CO}_2} \quad (\text{C3})$$

$$X_2 = N_{\text{CH}_4} + N_{\text{H}_2\text{O}} + N_{\text{CO}_2} \quad (\text{C4})$$


$$X_3 = N_{\text{H}_2} + N_{\text{CH}_4} + N_{\text{H}_2\text{O}} \quad (\text{C5})$$

$$X_4 = N_{\text{H}_2} + N_{\text{CH}_4} \quad (\text{C6})$$


Equation (C2) represents about 20% of total CH₄ photolysis.

ORCID iDs

Kevin J. Zahnle  <https://orcid.org/0000-0002-2462-4358>

Roxana Lupu  <https://orcid.org/0000-0003-3444-5908>

David C. Catling  <https://orcid.org/0000-0001-5646-120X>

Nick Wogan  <https://orcid.org/0000-0002-0413-3308>

- Abe, Y. 1997, *PEPI*, 100, 27
 Abe, Y., & Matsui, T. 1988, *JATS*, 45, 3081
 Abelson, P. H. 1966, *PNAS*, 55, 1365
 Agnor, C. B., & Asphaug, E. 2004, *ApJL*, 613, L157
 Ahrens, T. J., O'Keefe, J. D., & Lange, M. A. 1989, in *Origin and Evolution of Planetary and Satellite Atmospheres*, ed. S. K. Atreya, J. B. Pollack, & M. S. Matthews (Tucson, AZ: Univ. Arizona Press), 328
 Albarède, F., Ballhaus, C., Blichert-Toft, J., et al. 2013, *Icar*, 222, 44
 Anders, E. 1989, *Natur*, 342, 255
 Anders, E., & Owen, T. 1977, *Sci*, 198, 453
 Armstrong, K., Frost, D. J., McCammon, C. A., Rubie, D. C., & Ballaran, T. B. 2019, *Sci*, 365, 903
 Aulbach, S., & Stagno, V. 2016, *Geo*, 44, 751
 Benner, S. A., Bell, E. A., Biondi, E., et al. 2019a, *ChemSystemChem*, e1900035
 Benner, S. A., Kim, H. J., & Biondi, E. 2019b, *Life*, 9, 84
 Bermingham, K. R., Worsham, E. A., & Walker, R. J. 2018, *E&PSL*, 487, 221
 Botke, W. F., Walker, R. J., Day, J. M. D., Nesvorný, D., & Elkins-Tanton, L. 2010, *Sci*, 330, 1527
 Brassler, R., Mojzsis, S. J., Werner, S. C., Matsumura, S., & Ida, S. 2016, *E&PSL*, 455, 85
 Budde, G., Burkhardt, C., & Kleine, T. 2019, *NatAs*, 3, 736
 Canil, D. 2002, *E&PSL*, 195, 75
 Carlson, R. W., Brassler, R., Yin, Q.-Z., Fischer-Gödde, M., & Qin, L. 2018, *SSRv*, 214, 121
 Carlson, R. W., Garnero, E., Harrison, T. M., et al. 2014, *AREPS*, 42, 151
 Chase, M. W. 1998, *JPCRD*, 9, 1
 Choudhry, K. I., Carvajal-Ortiz, R. A., Kallikragas, D. T., & Svishchev, I. M. 2014, *Corros. Sci.*, 83, 226
 Chyba, C. F., & Sagan, C. 1992, *Natur*, 355, 125
 Claire, M. W., Sheets, J., Cohen, M., et al. 2012, *ApJ*, 757, 95
 Cleaves, H. J., Chalmers, J. H., Lazcano, A., Miller, S. L., & Bada, J. L. 2008, *OLEB*, 38, 105
 Curdt, W., Brekke, P., Feldman, U., et al. 2001, *A&A*, 375, 591
 Dauphas, N. 2017, *Natur*, 541, 521
 Dauphas, N., & Morbidelli, A. 2014, *Treatise in Geochemistry* (2nd ed.; Oxford: Elsevier) doi:10.1016/B978-0-08-095975-7.01301-2
 Day, J. M. D., Brandon, A. D., & Walker, R. J. 2016, *RvMG*, 81, 161
 Dean, A. M., & Bozzelli, J. W. 2000, in *Gas-Phase Combustion Chemistry*, ed. W. C. Gardiner, Jr. (Berlin: Springer), 125
 Delano, J. W. 2001, *OLEB*, 31, 311
 Dreibus, G., & Wänke, H. 1989, in *Origin and Evolution of Planetary and Satellite Atmospheres*, ed. S. K. Atreya, J. B. Pollack, & M. S. Matthews (Tucson: Univ. Arizona Press), 268
 Elkins-Tanton, L. 2008, *E&PSL*, 271, 181
 Elkins-Tanton, L., & Seager, S. 2008, *ApJ*, 685, 1237
 Ferris, J. F., Joshi, P. C., Edelson, E. H., & Lawless, J. G. 1978, *JMoIE*, 11, 293
 Fischer-Gödde, M., Burkhardt, C., Kruijer, T. S., & Kleine, T. 2015, *GeCoA*, 168, 151
 Fischer-Gödde, M., Elfers, B.-O., Münker, C., et al. 2020, *Natur*, 579, 240
 Fischer-Gödde, M., & Kleine, T. 2017, *Natur*, 541, 525
 Frost, D. J., & McCammon, C. A. 2008, *AREPS*, 36, 389
 Genda, H., Brassler, R., & Mojzsis, S. J. 2017a, *E&PSL*, 480, 25
 Genda, H., Iizuka, T., Sasaki, T., Ueno, Y., & Ikoma, M. 2017b, *E&PSL*, 470, 87
 Greenwood, R. C., Barrat, J.-A., Miller, M. F., et al. 2018, *SciA*, 4, eaao5928
 Haldane, J. B. S. 1929, *Rationalist Ann.*, 1929, 12
 Halliday, A. N. 2013, *GeCoA*, 105, 146
 Hashimoto, G. L., Abe, Y., & Sugita, S. 2007, *JGRE*, 112, E05010
 Heays, A. N., Visser, R., Gredel, R., et al. 2014, *A&A*, 562, A61
 Herron, J. T. 1999, *JPCRD*, 28, 1453
 Holland, H. D. 1964, in *The Origin and Evolution of Atmospheres and Oceans*, ed. P. J. Brancaccio & A. G. W. Cameron (New York: Wiley), 86
 Holland, H. D. 1984, *The Chemical Evolution of the Atmosphere and Oceans* (Princeton, NJ: Princeton Univ. Press)
 Hopp, T., & Kleine, T. 2018, *E&PSL*, 494, 50
 Hörst, S. M., He, C., Ugelow, M. S., et al. 2018, *ApJ*, 858, 119
 Hörst, S. M., Yelle, R. V., Buch, A., et al. 2012, *AsBio*, 12, 809
 Huebner, W. F., Keady, J. J., & Lyon, S. P. 1992, *Ap&SS*, 195, 1
 Johnson, A. P., Cleaves, H. J., Dworkin, J. P., et al. 2008, *Sci*, 322, 404
 Kasting, J. F. 1990, *OLEB*, 20, 199
 Kraus, R. G., Root, S., Lemke, R. W., et al. 2015, *NatGe*, 8, 269
 Kress, M. E., & McKay, C. P. 2004, *Icar*, 168, 475
 Kuhn, W. R., & Atreya, S. K. 1979, *Icar*, 37, 207

- Kuramoto, K. 1997, *PEPI*, **100**, 3
- Kuwahara, H., & Sugita, S. 2015, *Icar*, **257**, 290
- Lasaga, A. C., Holland, H. D., & Dwyer, M. J. 1971, *Sci*, **174**, 53
- Li, X., Heays, A. N., Visser, R., et al. 2013, *A&A*, **555**, A14
- Liang, M.-C., Heays, A. N., Lewis, B. R., Gibson, S. T., & Yung, Y. L. 2007, *ApJL*, **664**, L115
- Line, M. R., Vasisth, G., Chen, P., Angerhausen, D., & Yung, Y. L. 2011, *ApJ*, **738**, 32
- Lupu, R. E., Feldman, P. D., Weaver, H. A., & Tozzi, G.-P. 2007, *ApJ*, **670**, 1473
- Lupu, R. E., France, K., & McCandliss, S. R. 2006, *ApJ*, **644**, 981
- Marrero, T. R., & Mason, E. A. 1972, *JPCRD*, **1**, 2
- Marty, B. 2012, *E&PSL*, **313**, 56
- Matsui, T., & Abe, Y. 1986, *Natur*, **322**, 526
- Miller, S. L. 1953, *Sci*, **117**, 528
- Miller, S. L. 1955, *J. Am. Chem. Soc.*, **77**, 2351
- Miller, S. L., & Urey, H. C. 1959, *Sci*, **130**, 245
- Morbidelli, A., Nesvorný, D., Laurenz, V., et al. 2018, *Icar*, **305**, 262
- Nakajima, S., Hayashi, Y.-Y., & Abe, Y. 1992, *JAtS*, **49**, 2256
- Newsom, H. E., & Taylor, S. R. 1989, *Natur*, **338**, 360
- Nicklas, R. W., Puchtel, I. S., Ash, R. D., et al. 2019, *GeCoA*, **250**, 49
- Oparin, A. I. 1938, *Origin of Life* (New York: Dover)
- Oró, J., & Kamat, S. 1961, *Natur*, **190**, 442
- Oró, J., Miller, S. L., & Lazcano, A. 1990, *AREPS*, **18**, 317
- Pasek, M., & Lauretta, D. 2008, *OLEB*, **38**, 5
- Pavlov, A. A., Brown, L. L., & Kasting, J. F. 2001, *JGRA*, **106**, 1
- Pinto, J. P., Gladstone, G. R., & Yung, Y. L. 1980, *Sci*, **210**, 183
- Poole, J. H. J. 1951, *Sci. Proc. Roy. Dublin Acad.*, **25**, 201
- Powner, M. W., Gerland, B., John, D., & Sutherland, J. D. 2009, *Natur*, **459**, 239
- Prinn, R. G., & Barshay, S. S. 1977, *Sci*, **198**, 1031
- Prinn, R. G., & Fegley, B., Jr 1981, *ApJ*, **249**, 308
- Read, A. J. 1982, *J. Solution Chem.*, **11**, 649
- Ricardo, A., Carrigan, M. A., Olcott, A. N., & Benner, S. A. 2004, *Sci*, **303**, 196
- Robinson, T. D., & Catling, D. C. 2014, *NatGe*, **7**, 12
- Rollinson, H., Adetunji, J., Lenaz, D., & Szilas, K. 2017, *Litho*, **282**, 316
- Rubie, D. C., Jacobson, S. A., Morbidelli, A., et al. 2015, *Icar*, **248**, 89
- Rubie, D. C., Laurenz, V., Jacobson, S. A., et al. 2016, *Sci*, **353**, 1141
- Sagan, C., & Chyba, C. F. 1997, *Sci*, **276**, 1217
- Schaefer, L., & Fegley, B. 2007, *Icar*, **186**, 462
- Schaefer, L., & Fegley, B. 2010, *Icar*, **208**, 438
- Schaefer, L., & Fegley, B. 2017, *ApJ*, **843**, 120
- Sleep, N. H. 2016, *GGG*, **17**, 2623
- Sleep, N. H., & Zahnle, K. J. 2001, *JGR*, **106**, 1373
- Sleep, N. H., Zahnle, K. J., Kasting, J. F., & Morowitz, H. J. 1989, *Natur*, **342**, 139
- Stribling, R., & Miller, S. L. 1987, *OrLi*, **17**, 261
- Sugita, S., & Schultz, P. 2009, *GeoRL*, **36**, L20204
- Sutherland, J. D. 2016, *Angew. Chem. Int. Edit.*, **55**, 104
- Tian, F., Kasting, J. F., & Zahnle, K. J. 2011, *E&PSL*, **308**, 417
- Trail, D., Watson, E. B., & Tailby, N. D. 2012, *GeCoA*, **97**, 70
- Trainer, M. G., Pavlov, A. A., DeWitt, H. L., et al. 2006, *PNAS*, **103**, 18035
- Tremaine, S., & Dones, L. 1993, *Icar*, **106**, 335
- Tyburczy, J. A., Frisch, B., & Ahrens, T. J. 1986, *E&PSL*, **80**, 201
- Urey, H. C. 1952, *PNAS*, **38**, 351
- Varas-Reus, M. I., König, S., Yierpan, A., Lorand, J.-P., & Schoenberg, R. 2019, *NatGe*, **12**, 779
- Visscher, C., & Moses, J. I. 2011, *ApJ*, **738**, 72
- Walker, J. C. G. 1977, *Evolution of the Atmosphere* (New York: Macmillan)
- Walker, R. J. 2009, *ChEG*, **69**, 101
- Wang, J., Xiong, X., Takahashi, E., et al. 2019, *JGRB*, **124**, 4617
- Wänke, H., & Dreibus, G. 1988, *RSPTA*, **325**, 545
- Wolf, E. T., & Toon, O. B. 2010, *Sci*, **128**, 1266
- Wordsworth, R. 2016, *E&PSL*, **447**, 103
- Wordsworth, R., & Pierrehumbert, R. T. 2013, *Sci*, **339**, 64
- Yung, Y. L., & Pinto, J. P. 1978, *Natur*, **273**, 730
- Zahnle, K., & Sleep, N. 1997, in *Comets and the Origin and Evolution of Life*, ed. P. Thomas, C. F. Chyba, & C. P. McKay (2nd ed.; Berlin: Springer), **175**
- Zahnle, K., & Sleep, N. 2006, in *Comets and the Origin and Evolution of Life*, ed. P. Thomas et al. (2nd ed.; Berlin: Springer), **207**
- Zahnle, K. J. 1986, *JGR*, **91**, 2819
- Zahnle, K. J., Arndt, N., Cockell, C., et al. 2007, *SSRv*, **129**, 35
- Zahnle, K. J., Catling, D. C., & Gacesa, M. 2019, *GeCoA*, **244**, 56
- Zahnle, K. J., & Marley, M. S. 2014, *ApJ*, **797**, 41
- Zahnle, K. J., & Walker, J. C. G. 1982, *RvGSP*, **20**, 280
- Zel'dovich, Ya. B., & Raizer, Yu. P. 1967, *Physics of Shock Waves and High Temperature Hydrodynamic Phenomena* (New York: Academic)